Response to Anonymous Referee 1 on "Measurement of ammonia, amines and iodine species using protonated water cluster chemical ionization mass spectrometry"

We thank the referee for the constructive comments that help improving our manuscript. In the following, the comments of the referee are shown in black, shaded font. Our replies are shown in blue font. Text that has been added or revised in the manuscript is shown in red font. In addition to the changes proposed by the reviewer, we have also added linguistic changes to the manuscript that do not change the content. These are listed after the answers to the reviewer, whereby we list the sentence previously used first.

Lines 306-307: The Authors should be clear that the data is not shown in the Figure. Where the response times corresponding to the Figure are discussed (Lines 309-312), it may be easier to relate between the two if the response times are reported in minutes (consistent with the x-axis in the figure).

We agree with the referee that a clearer distinction between the response times discussed in Section 3.3 is helpful to improve understanding this Section of the manuscript. Thus, we changed the text in our Section 3.3 to distinguish in a more clear way between the response times shown in the Figure and the response times reported in the text. Next to this, we changed the unit of our x label in the Figure towards "seconds" to stay consistent with the text.

We define the response time as the time required for the instrument to reach 95% of the new mixing ratio being injected. The response time takes into account two processes. It includes both the response time of the instrument ("instrumental response time") and the time for the lines to reach a steady state for ammonia delivery ("line response time"). Figure 4 indicates the typical response times of the water cluster CI-APi-TOF during calibrations (here at 60% relative humidity). It shows a decay between two calibration steps when the injected ammonia is reduced from 9509 pptv to 6911 pptv and a rise in the signal when the ammonia mixing ratio is increased from 500 pptv to 9509 pptv. Panel a) indicates a clear difference between the fast instrumental response time (red line) and the slower line response time (black line). While we expect a similar behavior in instrumental response time for a decay from 9509 to 500 pptv, a longer line response time is expected due to re-evaporation of ammonia from the sampling lines. Thus, the mixing ratios were gradually reduced during calibrations. The instrumental response time shown in Figure 4 is at 6 s for a decay in mixing ratio (9509 pptv to 6911 pptv) and at 18 s for a rise (500 pptv to 9509 pptv). The line response time is at 37 s (decay) and at 890 s (rise). The difference between the short line response time for a decay in ammonia mixing ratio compared to a rise The experiments were repeated several times at varying relative humidies.

The instrumental response time only varied by a few seconds during our experiments (between 6 to 10 s (decay) and 18 to 25s (rise)). While the variation in instrumental response time is small, the line response time can vary strongly depending on precursor conditions and relative humidity. During our experiments, the line response time varied between 37 s and 54 s (decay) and between 535 s and 890 s (rise) respectivelly. Interactions of ammonia with the sampling line are discussed in Section 3.8.

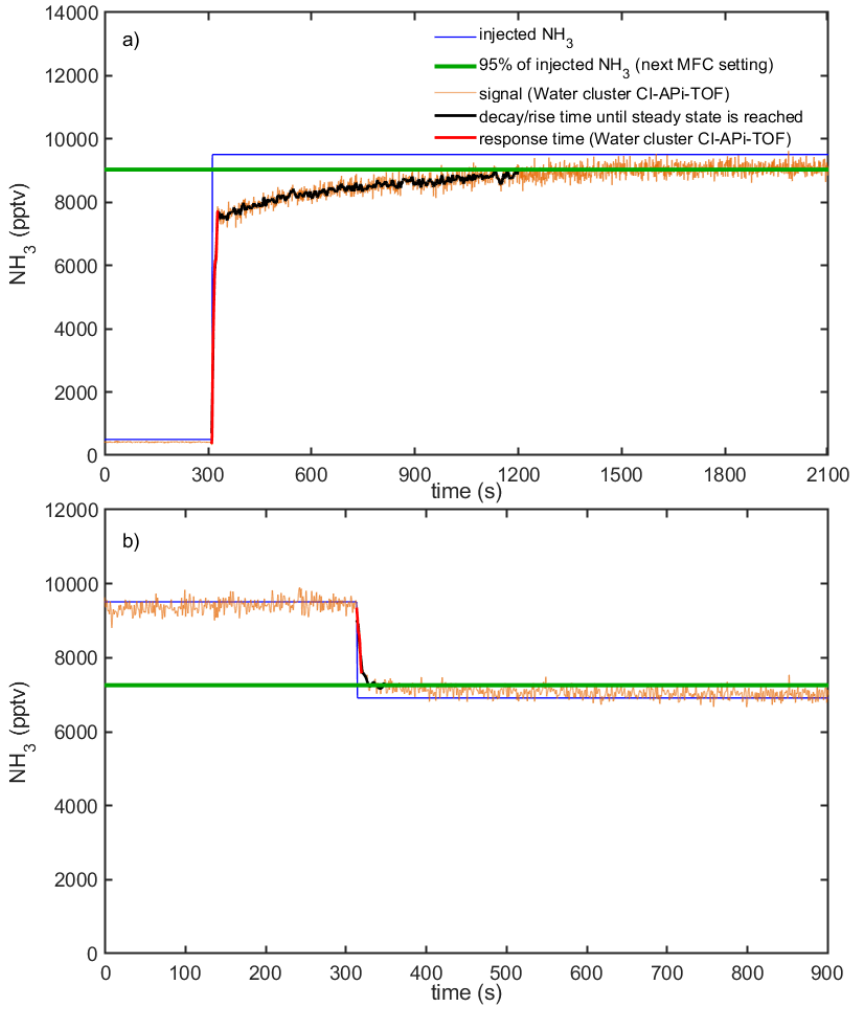

Figure 4: Response time of the water cluster CI-APi-TOF during calibrations at 60% RH. The injected ammonia mixing ratio from MFC settings is shown by the blue line. The signal of the water cluster CI-APi-TOF is shown by the orange line (here the data are shown with a 1 second time resolution i.e. no time-averaging is applied). The green line represents 95% of the mixing ratio being applied with the next MFC setting. The black line shows the response time until a steady state (panel a) or 95% of the final measured concentration is reached (panel b). The response time is the sum of the response time of the water-cluster CI-APi-TOF (red line) and the (slower) response time for the lines to reach a steady state where the walls are conditioned.

Line 373: There is a citation formatting issue here for von Bobutzki et al, with the 'von' missing.

We updated the text according to the comment of the referee. Next to this, we replaced "in any case" by "nevertheless":

Nevertheless, the detection limit derived for ammonia is well below the LOD reported for other measurement techniques and instruments (von Bobrutzki et al., 2010; You et al., 2014; Lin; Wang et al., 2015).

Section 3.7: The discussion here is, generally, quite well presented. One detail remains, however, regarding the comparison of the PICARRO against the CI-APi-TOF due to reporting NH3 measurements from the PICARRO well below its detection limit (stated as 366 pptv on Line 237). At Line 419, the 'background' for the PICARRO is reported as ~200 pptv, but this is lower than its detection limit. This should be replaced with a statement clearly stating that the backgrounds were below the detection limit. This same approach is necessary in discussing the detection of NH3 by the PICARRO in the subsequent comparison. Where PICARRO NH3 is less than 366 pptv, the discussion should not comment on the performance of the instrument as it cannot detect such levels (e.g. 'can hardly detect this decrease in the VMR' on Lines 428-429 and again in the last sentence of the section at Lines 449-450). Likewise, NH3 data from the PICARRO that is below the LOD should either not be presented in Figures 8a and 8b or a horizontal line on the plot denoting the PICARRO LOD should be provided so readers are not expecting more from this instrument.

We changed our Section 3.7 according to the comments from the Referee. The detection limit stated as 366 pptv was determined during the CLOUD13 campaign (during the same time where we determined the detection limit of the water cluster CI-APi-TOF). In Section 3.7, we show a longterm timeseries from the CLOUD12 campaign (one year before). We determined the detection limit at this time to be at 170.1 pptv. On Line 231 (Section 2.4) we added the detection limit during the CLOUD12 experiments to the description of the PICARRO:

By using the same method (at the same time period) as for the water cluster CI-APi-TOF (see Section 3.5), we derive a detection limit of 366.2 pptv for the PICARRO unit used in our study during CLOUD13. The detection limit derived for the PICARRO used during the CLOUD12 experiments is at 170.1 pptv.

Next to this, we updated the text in Section 3.7 on Line 408 of our updated manuscript, where we initially stated:

"Figure 8a shows the measurements of the water cluster CI-APi-TOF, the PICARRO, and the calculated value for ammonia. The signal measured by the water cluster CI-APi-TOF follows the injected ammonia almost instantaneously (first injection is on Oct. 23), whereas the PICARRO only shows elevated concentrations above its background of ~200 pptv much later."

The updated text is shown below:

Figure 8a shows the measurements of the water cluster CI-APi-TOF, the PICARRO and the calculated value for ammonia. The PICARRO trace is shown for the time when the detection limit (170.1 pptv during CLOUD12) is exceeded. The signal measured by the water cluster CI-APi-TOF follows the injected ammonia almost instantaneously (first injection is on Oct. 23).

The initial aim behind commenting on the PICARRO measurements below its detection limit was to explain deviations between the instruments at low mixing ratios of ammonia. Nevertheless, we agree with the Referee that stating the detection limit of the PICARRO in the beginning of the Section already explains deviations between the instruments at low concentrations. Thus, we removed the sentence on line 428-429 (previous manuscript): "Due to the higher LOD, the PICARRO, however, can hardly detect this decrease in the VMR."

In order to bring the following sentence back into context with the text ("*This increased response time can be explained by a combination of the longer sampling line (~1.8 m compared to 1.3 m for the water cluster CI-APi-TOF), the lower flow rate (~ 1 slm with a core sampling of 5 slm compared with ~ 20 slm for the water cluster CI-APi-TOF) and the higher detection limit of the PICARRO.*"), we have changed it slightly:

The slower response time of the PICARRO can be explained by a combination of the longer sampling line (~1.8 m compared to 1.3 m for the water cluster CI-APi-TOF) and the lower flow rate (~ 1 slm with a core sampling of 5 slm compared with ~ 20 slm for the water cluster CI-APi-TOF).

In the last sentence of the Section, we now explain why the PICARRO trace is not shown in Figure 8b (since the mixing ratios are below the LOD of the PICARRO):

Due to its higher detection limit, the PICARRO is insensitive at these low mixing ratios (green line in Figure 8b).

We updated Figure 8 according to the comments of the Referee, where we removed the PICARRO trace below its detection limit and where we added a line stating the detection limit of the PICARRO in Figure 8b instead:

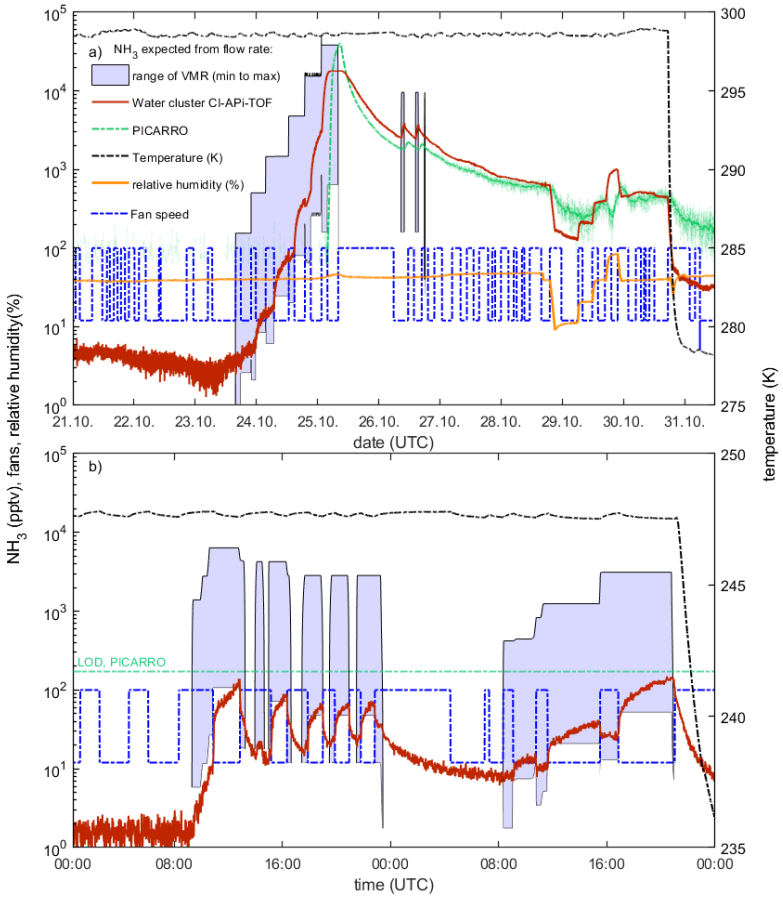

Figure 6: The temperature color scale can be removed as only two temperatures are on this figure. The corresponding T values can be added to the caption and/or the legend for each of the three data series.

We agree with the Referee that adding the temperature to the caption and removing the color scale improves legibility since only two temperatures are shown. Thus, we updated our Figure 6 as shown below:

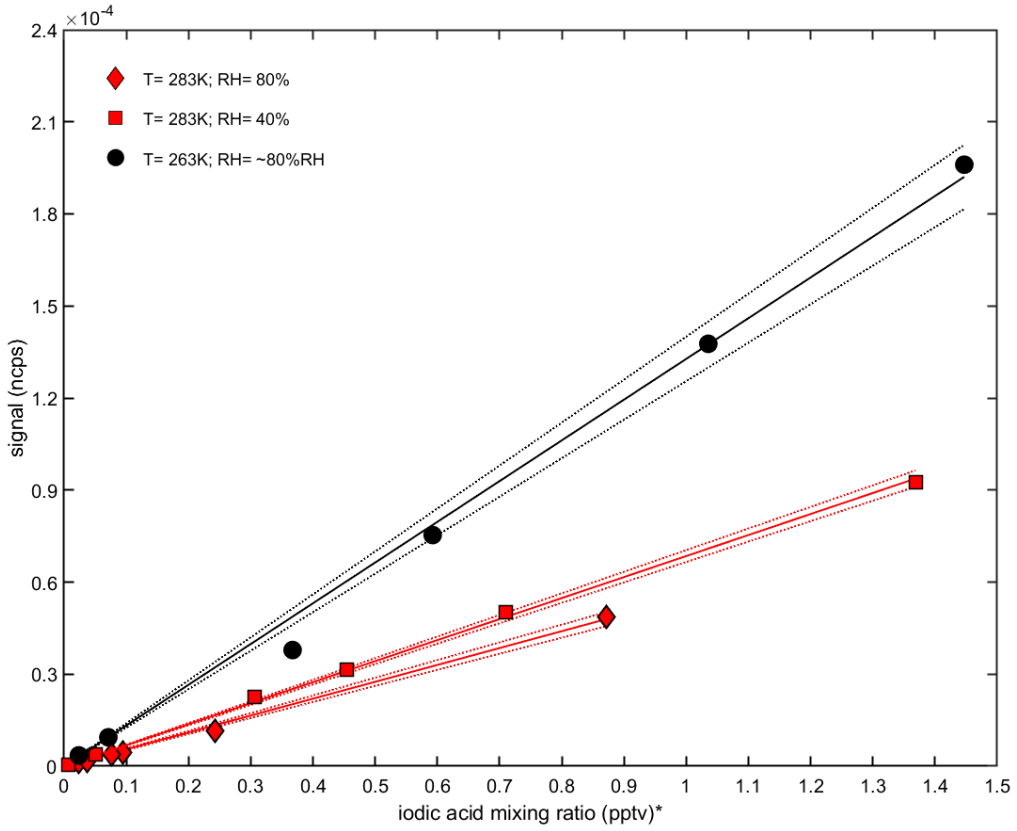

Figure 7: Should the 'primary ions' here be 'reagent ions' in order to be consistent with the figure caption?

Using ‘reagent ions’ in Figure 7 instead of ‘primary ions’ makes sense to stay consistent with our caption and text. Thus, we updated Figure 7:

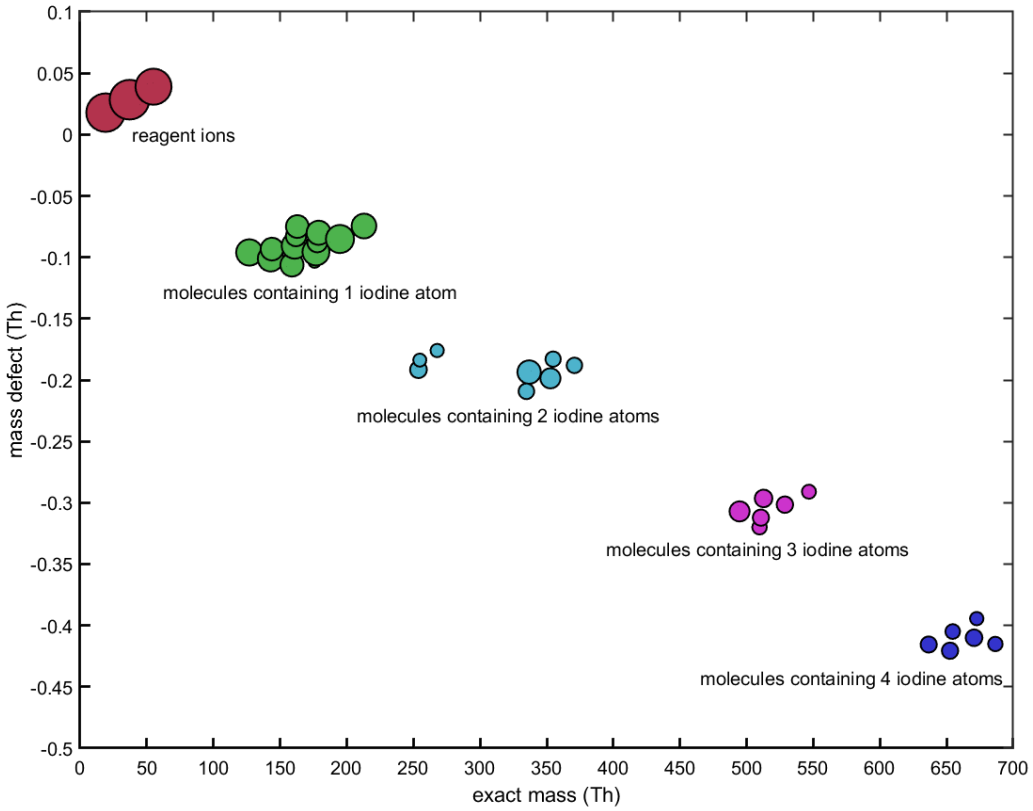

Next to the changes suggested by the Referee, we tried to improve the legibility of our manuscript. The content has not been changed. Since all changes are minor text corrections, we don't comment on the changes made. The original sentences from our previous manuscript are shown in shaded, blue font, the updated sentences are shown in shaded, red font.

Since we use "compounds" instead of "species" throughout the manuscript, we would like to change the title from:

"Measurement of ammonia, amines and iodine species using protonated water cluster chemical ionization time of flight mass spectrometry".

Towards:

"Measurement of ammonia, amines and iodine compounds using protonated water cluster chemical ionization time of flight mass spectrometry".

We changed our Figure 1, where we adjusted Panel b) so, that the ion source has the same orientation as shown in Panel a. Next to this, we changed the color of the arrows pointing towards the ion source to improve the clarity of the figure. We added an elipse around the ion source in Panel a and an arrow to connect the two panels with each other:

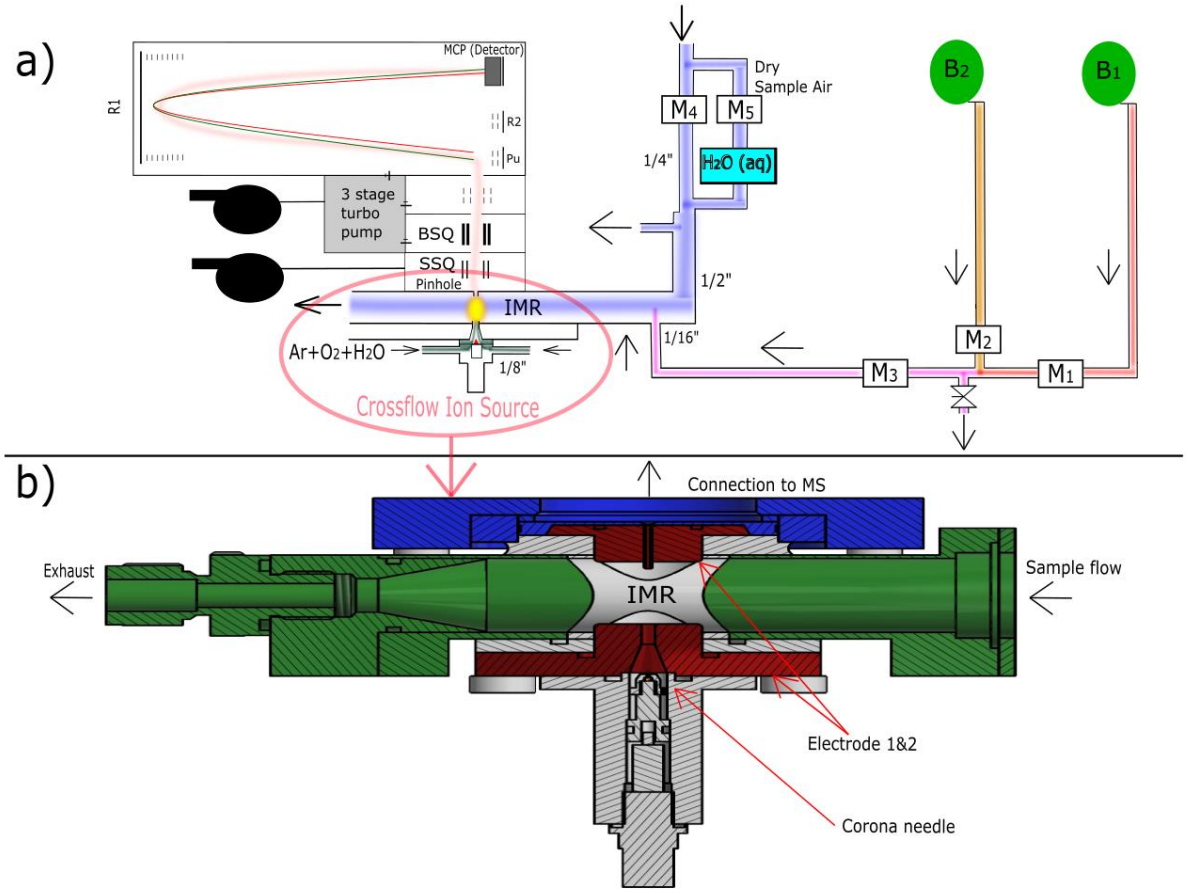

Line 19:

[…] at the CLOUD (Cosmics Leaving OUtdoor Droplets) […].

[…] at the CERN CLOUD (Cosmics Leaving OUtdoor Droplets) […].

Line 21-23:

Due to a short ion-molecule reaction times (< 1ms) and high reagent ion concentrations ammonia mixing ratios of at least up to 10 ppbv can be measured without significant reagent ion depletion.

Due to the short ion-molecule reaction time and high reagent ion concentrations, ammonia mixing ratios up to at least 10 ppbv can be measured with the instrument without significant saturation due to reagent ion depletion.

Line 51-53:

For these reasons the measurement of these compounds is required in order to understand new particle formation and the partitioning between the gas and aerosol phase. It is important to note that ammonia can easily exceed several ppbv in the boundary layer, whereas amine mixing ratios are typically present at a few pptv only.

For these reasons improved gas-phase measurements of these compounds are required. Sensitive real-time measurements are needed spanning mixing ratios over a broad atmospheric range between a few pptv to a few ppbv of ammonia in the boundary layer, and around a few pptv of amines.

Line 65:

The limit of detection (LOD) varies between […]

The reported limits of detection (LOD) varies between […]

Line 76:

Besides measurement of basic compounds with high proton affinity, we have discovered that the protonated water clusters […]

Besides measurement of basic compounds with high proton affinity, we find that the protonated water clusters […]

Line 112:

[….] ambient temperature of ~20 °C.

[…] ambient temperature of near ~20 °C.

Line 115:

[…] for oxygen were used, respectively.

[…] for oxygen were used.

Line 116:

First attempts have been made using nitrogen instead of argon […]

Initially we used nitrogen instead of argon […]

Line 117:

These backgrounds are most likely explained by NH_3 production involving N_2 in the corona plasma.

This is likely due to NH_3 production in the corona plasma when nitrogen is present.

Line 122:

[…] formation of protonated water clusters is shown below

[…] formation of protonated water clusters is shown as follows

Line 131:

[…] to break up water clusters such that mainly H_3O^+ ions react.

[…] to break up water clusters so that mainly non-hydrated H_3O^+ ions remain.

Line 139:

As water molecules can evaporate […]

Since water molecules can evaporate […]

Line 140

[…] some of the product ions can be detected […]

[…] some of the product ions are detected […]

Line 170:

A calibration factor, C, that includes factors […]

A calibration factor, C, which includes factors […]

Line 185-186:

Figure 1a shows a schematic drawing of the experimental setup during the calibrations with ammonia. The ammonia was taken from a gas bottle containing an NH_3 mixing ratio, B, of 100 ppmv diluted in pure nitrogen (Air Liquide, ±5% uncertainty for the certified NH_3 mixing ratio) that is diluted in two steps[…]

During calibrations, ammonia was drawn from a gas bottle containing an NH_3 mixing ratio, B, of 100 ppmv diluted in pure nitrogen (Air Liquide, ±5% uncertainty for the certified NH_3 mixing ratio). It was diluted in two steps […]

Line 193:

The flow of ammonia from the gas bottle is described by M_1 […]

The flow of ammonia from the gas bottle is set by M_1[…]

Line 195:

[…]the same synthetic air that is used for the CLOUD chamber.

[…]the same synthetic air as used for the CLOUD chamber.

Line 201:

To obtain calibration curves, the highest targeted ammonia mixing ratio is adjusted first. The calibration points are then recorded by stepping down the flow of M_3. In this way, equilibration times are fairly short as the NH_3 mixing ratio before and directly after M_3 remains constant (see also Section 3.2).

In Section 3.2 we repeat the statement mentioned above. Thus, we decided to remove it here and refer to Section 3.2 instead:

Results of the calibrations are discussed in Section 3.2.

Line 203-205:

Besides the detection of ammonia and dimethylamine by the described ionization scheme, product ions from iodine-containing species were detected during new particle formation experiments initiated from I_2 photolysis during the CLOUD13 run. Prominent signals ($HIO_3 \cdot H^+$ and $HIO_3 \cdot H_3O^+$) corresponding to the neutral species of HIO_3 were observed among others (discussed in Section 3.6 and Table 2).

The water cluster chemical ionizer is also effective for iodine-containing species, which were detected in new particle formation experiments from I_2 photolysis during CLOUD13. Prominent signals of iodic acid ($HIO_3 \cdot H^+$ and $HIO_3 \cdot H_3O^+$) were observed among many iodine compounds (Section 3.6 and Table 2).

Line 208-209:

[…] another chemical ionization mass spectrometer using nitrate reagent ions (nitrate CI-APi-TOF) was also measuring HIO_3 at CLOUD.

[…]a second chemical ionization mass spectrometer at CLOUD, using nitrate reagent ions (nitrate CI-APi-TOF), was also measuring HIO_3 simultaneously.

Line 209-210:

[…]a calibration factor for HIO_3 is derived […], that is calibrated for sulfuric acid […]

[…]a calibration factor for HIO_3 has been derived […] , which itself had been calibrated for sulfuric acid […]

Line 212:

However, as the reaction of sulfuric acid with nitrate ions is at the kinetic limit, the detection limits […]

However, as the reaction of sulfuric acid with nitrate ions is at the kinetic limit (Viggiano et al., 1997), the detection limits […]

Line 214-215:

[…]Thus, the applied assumption in the present study was also used in a previous study for deriving gas phase concentrations of iodic acid (Sipilä et al., 2016).

[…]The assumption we use in the present study was also applied in a previous study for deriving gas phase concentrations of iodic acid (Sipilä et al., 2016).

Line 217:

[…] experimental runs were chosen […]

[…] experimental runs were selected […]

Line 220-221:

A PICARRO G1103-t NH_3 Analyzer (PICARRO Inc., USA) measured ammonia mixing ratios based on based on cavity-ring down spectroscopy during CLOUD12 and CLOUD13.

A PICARRO G1103-t NH_3 Analyzer (PICARRO Inc., USA) measuring ammonia mixing ratios based on cavity-ring down spectroscopy was also connected to the CLOUD chamber during CLOUD12 and CLOUD13.

Line 226:

[…]to minimize line losses and to decrease the response times.

[…]to minimize line losses and to shorten the response time.

Line 230:

[…]a lower detection limit of 200 pptv is reported […]

[…]a lower detection limit of 200 pptv is specified […]

Line 236:

$(H_2O)H_3O^+$ is the dominant primary ion in the mass spectrum.

The dominant primary ion is $(H_2O)H_3O^+$.

Line 238-239:

[…]the signal from NH_4^+ can have a similar magnitude compared with the signal from H_2O^+ (possibly from reactions of O_2^+ and H_2O).

[…]the signal from NH_4^+ has a similar magnitude as H_2O^+ (which may arise from reactions of O_2^+ with H_2O).

Line 240:

[…]is essential in terms of reaching low detection limits […]

[…]is essential to reach low detection limits for ammonia […]

Line 241:

At the low masses the APi-TOF used in the present study reaches a resolving power of ~2000 Th/Th […]

At low mass the APi-TOF used in the present study has a resolving power of ~2000 Th/Th […]

Line 244:

Prominent peaks from N_2H^+, NO^+ and O_2^+ can also be found in the spectrum shown in Figure 2.

Prominent peaks from N_2H^+, NO^+ and O_2^+ are also seen (Figure 2).

Line 246:

[…] as reagent ions (in equation (1)) as no evidence exists that they interact […]

[…] as reagent ions (in equation 1) as we have no indication that they interact […]

Line 248:

[…]; but NH_3^+ is not considered […]

[…]; however NH_3^+ is not considered […]

Line 252-253:

For estimating an ammonia mixing ratio according to equation (1), the product ion count rates are normalized against the dominating reagent ion count rates.

For estimating an ammonia mixing ratio (Equation 1), the signal ion count rates are normalized to the dominating reagent ion count rates.

Line 253-254:

[…]the reagent ion signals are significantly higher than the product ion count rates.

[…] the reagent ion signals are an order of magnitude higher than the signal ion count rates.

Line 254-255:

This indicates that no significant reagent ion depletion occurs and thus the normalized counts per second respond linearly with the ammonia VMR […]

This indicates that very little reagent ion depletion occurs and thus the normalized counts per second are linear with the ammonia mixing ratio […]

Line 257:

Figure 3 shows the calibration curves obtained for NH_3 and HIO_3 (for the CLOUD13 campaign).

Figure 3 shows the calibration curves obtained for NH_3 and HIO_3 during the CLOUD13 campaign.

Line 259-260:

(ammonia: NH_4^+ and $(H_2O)NH_4^+$; iodic acid: HIO_3H^+ and $HIO_3H_3O^+$).

(NH_4^+ and $(H_2O)NH_4^+$ for ammonia and HIO_3H^+ and $HIO_3H_3O^+$ for iodic acid).

Line 260-261:

[…]VMR (on the x-axis)[…] and the uncertainty of the VMR inside the ammonia gas bottle.

[…]mixing ratio (x-axis) […] and the uncertainty of the ammonia gas bottle concentration.

Line 269-271:

The calibration was performed before the CLOUD13 experiment (Sept. 2018), during and after the experiment (Dec. 2018) at different levels of humidity (calculated relative humidity levels between ~3% and 82%) and ambient temperatures.

The calibration was performed in September 2018, before the CLOUD13 campaign and also during and after the end of the campaign in December at relative humidties between ~3% and 82% and at ambient temperatures of the experimental hall near 293K.

Line 278-279:

For this reason, we derived the limit of detection by measuring the background of the CLOUD chamber with the calibration lines removed (Section 3.5).

We therefore derived the limit of detection by measuring the ammonia background in the CLOUD chamber with the calibration lines disconnected from our instrument (Section 3.5).

Line 280:

[…]the water reservoir is saturated with water (Figure 1a).

[…]the water reservoir is 100% saturated (Figure 1a).

Line 308:

Figure 5 shows the sensitivity dependence for the ammonia measurements with varying relative humidity.

Figure 5 shows the sensitivity of the ammonia measurements to relative humidity.

Line 308-309:

These data points are derived from calibration curves similar to the one shown in Figure 3a. However, during the calibrations […]

These data are derived from calibration curves similar to that of Figure 3a. During the calibrations […]

Line 317:

[…] the observed increase in sensitivity is not dramatic […]

[…], the observed increase in sensitivity is modest[…]

Line 320:

[…]our calibration setup is not temperature-controlled.

[…]our calibration setup was not temperature-controlled.

Line 320-321:

However, during a transition from high to low temperature in the CLOUD chamber […]

However, during a transition from 298K to 248K in the CLOUD chamber […]

Line 323:

The dependency of the sensitivity with relative humidity and temperature is different for the measurement of iodic acid as shown in Figure 6.

For iodic acid measurements, the sensitivity to relative humidity and temperature is different (Figure 6).

Line 324-325:

While NH_4^+, without a water molecule, is the dominant signal for ammonia, $H_4IO_4^+$, which is $H_2O{\cdot}HIO_3H^+$ or $HIO_3{\cdot}H_3O^+$, yields the highest signal for iodic acid.

While NH_4^+, without any water molecule, is the dominant signal for ammonia, the highest iodic acid signal is $H_4IO_4^+$, which is $H_2O{\cdot}HIO_3H^+$ or $HIO_3{\cdot}H_3O^+$.

Line 326:

The higher count rate of $H_4IO_4^+$ compared to $H_2IO_3^+$ could indicate that […]

The higher counting rate of $H_4IO_4^+$ compared to $H_2IO_3^+$ indicates that […]

Line 329:

[…]in a non-equilibrium process.

[…]in a non-equilibrium state.

Line 330:

These species are listed in Table 2.

These compounds are listed in Table 2.

Line 330-331:

Elucidating the exact formation pathways of these ions and the corresponding neutral species is subject for future work.

Elucidating the formation pathways of these ions and the corresponding neutral species is a subject for future work.

Line 333:

Determining the limit of detection (LOD) for ammonia is not trivial as the background signal is not constant.

Determining the limit of detection (LOD) for ammonia is complicated by changes in the observed background signal.

Line 334:

[…]background was observed, which was usually decreasing slowly after the ammonia flow[…]

[…]background was measured, which was decreasing slowly after the ammonia flow[…]

Line 336:

[…] signals usually dropped significantly […]

[…] signals usually fell more rapidly […]

Line 337-339:

However, even under these conditions the ammonia was not zero and the measured signal changed when the RH or temperature of the chamber was adjusted.

However, even under these conditions the ammonia was not zero and the measured signal changed when the RH or temperature of the chamber was adjusted, indicating the release of ammonia from the chamber walls.

Line 339-340:

There is evidence that the contaminant level of the CLOUD chamber with respect to ammonia is on the order of several pptv at 278 K and 38% RH (Kürten et al., 2016a).

The ammonia contaminant level of the CLOUD chamber was previously determined to be several pptv at 278 K and 38% RH (Kürten et al., 2016a).

Line 340-341:

During CLOUD13 the measured background (at 278 K and 80% RH) was 3.7 pptv, which in principle confirms the previous estimates.

During CLOUD13 the measured ammonia background was 3.7 pptv at 278 K and 80% RH, which confirms the previous estimates made with less sensitive ammonia instrumentation.

Line 341-342:

The fact that the sampling line of the instrument can also be a source of contamination could explain the somewhat higher value.

The measured background also includes any contamination in the sampling line of the instrument.

Line 345:

However, replacing nitrogen with argon quite drastically decreased […]

Replacing nitrogen with argon sharply decreased […]

Line 346-347:

Still, traces of nitrogen containing gases in the ion source could contribute to the ammonia background.

Nevertheless, traces of nitrogen-containing gases in the ion source could potentially contribute to the ammonia background.

Line 347-348:

For the present study we report a background ammonia mixing ratio of 3.7 pptv (Table 1) for 278 K and 80% RH but note that the background is significantly lower for lower chamber temperatures, which argues against the ion source being a significant source of ammonia since it is always at ambient temperature.

However the ammonia background reduces at lower chamber temperatures, which argues against the ion source being a significant source of ammonia.

Line 349-350:

[…] ratio that is necessary to exceed three times the standard deviation at background conditions […]

[…] that is necessary to exceed three standard deviations of the background fluctuations […]

Line 351-352:

[…]LODs for other compounds can be estimated.

[…]we can estimate LODs for other compounds.

Line 353-354:

[…]The evaluation of high resolution data is necessary for deriving the values shown in Table 1 as for some compounds several species occur at the same integer mass.

[…]High resolution data are necessary to reach the LODs shown in Table 1 since several species may share the same integer mass.

Line 356-357:

[…] even when using high resolution data.

[…], even with high resolution data.

Line 358-360:

However, the effect is small as the ion signals with the associated water are smaller than the products without the water molecule for the measured bases. The goodness of the assumption (using the calibration constant derived for ammonia for dimethylamine) is discussed in Section 3.9.

However, the effect is small since for the measured bases, the ion signals with associated water are smaller than the products without the water molecule. The goodness of the assumption of using the same calibration constant for dimethylamine as that derived for ammonia is discussed in Section 3.9.

Line 362-363:

This might be the case, since low levels of NH_3 are more difficult to achieve due to the ubiquitous presence of ammonia. In any case, […]

Ammonia is ubiquitous and hard to remove completely by water purification systems, so it can be introduced into the CLOUD chamber via the air humidification system. Nevertheless, […]

Line 366:

The signal of dimethylamine is most of the time below the estimated limit of detection.

The dimethylamine level in the CLOUD chamber is mostly below the estimated LOD.

Line 367:

The estimated detection limit of iodic acid is well below the LOD calculated for ammonia and dimethylamine (Table 1).

The estimated LOD of iodic acid is well below that of ammonia and dimethylamine (Table 1).

Line 374: We changed the title of Section 3.6 from "Identified iodine species during CLOUD13" to:

3.6 Iodine species identified during CLOUD13

Line 375-376:

The signals for HIO_3 measured by the water cluster CI-APi-TOF show an excellent correlation with the iodic acid concentration from the nitrate CI-APi-TOF measuring in negative ion mode (see Figure 3b). Additionally, […]

The CI-APi-TOF measurements of HIO_3 with positive water cluster ionization show excellent correlation with negative nitrate ionization (Figure 3b). Furthermore, […]

Line 377:

[…] during several experimental runs.

[…]during several experiments.

Line 377-380:

Figure 7 shows the detected iodine species during an experimental run, when a high iodine concentration was injected into the chamber (mean values over a duration of 120 minutes). The derived mean iodic acid mixing ratio is ~0.98 pptv according to the measurements of the water cluster CI-APi-TOF. During this time period, we observed compounds containing up to 4 iodine atoms.

Figure 7 shows the detected iodine species when a high iodine concentration (~50-100pptv) was injected into the chamber (mean values over a duration of 120 minutes). The derived mean iodic acid mixing ratio is ~0.98 pptv according to the measurements of the water cluster CI-APi-TOF. During this experiment, we observed compounds containing up to 4 iodine atoms.

Line 380:

The size of the circles shown in Figure 7 corresponds to […]

The size of the circles in Figure 7 corresponds to […]

Line 381-382:

To provide more details on the observed signals, Table 2 lists the sum formulas of some identified iodine species.

Table 2 lists the sum formulas of some identified iodine species during this experiment.

Line 383-384:

During some runs, an electric field was applied to the chamber to get rid of ions and cluster ions for the study of purely neutral (i.e., uncharged) nucleation.

During some experiments, an electric field of about 20 kV/m was applied in the chamber to remove ions and study purely neutral (i.e., uncharged) nucleation.

Line 384:

Even during these experiments the signals as displayed in Figure 7 were present.

Even during these experiments, the same signals as shown in Figure 7 were present.

Line 386:

[…] overview of the iodine signals observed so far with […]

[…] overview of the iodine signals measured with […]

Line 390:

[…] during measurements at CLOUD12 is shown in Figure 8.

[…] during CLOUD12 experiments with ammonia is shown in Figure 8.

Line 391-392:

In addition, both measurements are compared with an estimated range of ammonia mixing ratios based on the injected amount of NH_3 into the CLOUD chamber […]

In addition, both can be compared with the range of ammonia mixing ratios expected from the MFC settings for ammonia injected into the CLOUD chamber […]

Line 394:

While the injected ammonia can easily be determined from the MFC settings, […]

While the injected ammonia can be determined to better than 20% from the MFC settings, […]

Line 395-396:

[…] the chamber walls can essentially represent a perfect sink and the ammonia has a short life time.

[…] the chamber walls represent a perfect sink and the ammonia has a short life time.

Line 397-398:

Measurements of sulfuric acid at different fan speeds suggest a change of a factor of 4 in the mixing ratios when the fan speed is changed from 12% to 100%.

Measurements with sulfuric acid indicate a factor of 4 increase of the wall loss rate when the fan speed is changed from the nominal setting of 12% to 100%.

Line 400-401:

[…] have been exposed for a long time with ammonia they reach eventually an equilibrium where condensation and evaporation rates become balanced.

[…] have been exposed for sufficient time with ammonia they reach an equilibrium where condensation and evaporation rates are equal.

Line 412:

[…] values when the chamber is being cleaned.

[…]values as the chamber progressively releases ammonia from the walls.

Line 414:

Whether this is due to the chamber, the instrument or the sampling line becoming cleaner is unclear.

Whether this is due to a gradual cleaning of the chamber, the instrument or the sampling line is unclear.

Line 415-416:

Figure 8a also indicates the influence of temperature on the background ammonia level.

Figure 8a also indicates the influence of temperature on the level of contaminant ammonia level, after ammonia had been injected into the chamber.

Line 416-417:

When the chamber temperature drops from 298 K to 278 K (shortly before Oct. 31) the residual NH_3 decreases by around a factor of 5, which is caused by a reduction in the re-evaporating ammonia from the chamber walls.

When the chamber temperature falls from 298 K to 278 K (shortly before Oct. 31) the contaminant NH_3 decreases by around a factor of 5 due to the lower evaporation rate of ammonia from the chamber walls.

Line 418-420:

The influence of relative humidity on the gas phase concentration of ammonia is shown (time from 29.10. to 30.10.). In addition to the change in sensitivity with relative humidity shown for the water cluster CI-APi-TOF (Section 3.4), a change in humidity can lead to an increased ammonia mixing ratio in the gas phase. This is due to the fact that water molecules can displace adsorbed ammonia on surfaces (Vaittinen et al., 2014).

The influence of changing relative humidity can be seen in Figure 8 between 29.10. and 30.10. Part of the change is due to the response of the water cluster CI-APi-TOF (Section 3.4). A second contribution arises since water molecules can displace adsorbed ammonia on surfaces (Vaittinen et al., 2014).

Line 426-431:

The time from 25.10 to 26.10 shows a steep increase in the PICARRO trace, while the ammonia trace derived from the water cluster CI-APi-TOF flattens out at 20 ppbv of ammonia. This indicates that the primary ions of the water cluster CI-APi-TOF are depleted at high vapor concentrations. It is important to mention that not only ammonia concentrations were elevated at this time, but also other vapor concentrations were rather high. During the CLOUD13 campaign, where a revised version of the ion source was used (see Section 3.2), the significant depletion of primary ions has been observed only at ammonia mixing ratios of 40 ppbv.

In Figure 8 during the early part of 25.10 the PICARRO shows a steep increase of ammonia while the water cluster CI-APi-TOF saturates near 20 ppbv, due to depletion of the primary ions. It is important to note that other vapor concentrations were also high at this time, which contributed to the depletion of the primary ions. During CLOUD13, where an improved version of the ion source was used (Section 3.2), significant depletion of primary ions was only observed above 40 ppbv ammonia.

Line 431:

[…]ammonia mixing ratios inside the CLOUD chamber react on changes of the fan speed.

[…] ammonia mixing ratios vary with the mixing fan speed in the CLOUD chamber.

Line 432-433:

[…] As the temperature in this example is low (248 K) and the chamber is rather clean the walls act as a perfect sink for ammonia.

[…] Since the temperature during these experiments was low (248 K), the chamber walls act as a fairly efficient sink for ammonia.

Line 433-434:

Therefore, the measured mixing ratios almost instantaneously react to the changing fan speed indicating a change of a factor 4 in the mixing ratios.

Therefore, the measured mixing ratios respond promptly to the changing fan speed indicating a change of almost a factor 4 in ammonia.

Line 434-436:

Thus, the measurements coincide with the calculated values using the wall loss life times reported above.

Moreover the measurements coincide with the values calculated from the MFC settings, assuming wall loss lifetimes of 100 s and 25 s at 12% and 100% fan speed, respectively.

Line 438-442:

At CLOUD, the sampling line is made of stainless steel and is kept as short as possible. The total length is still 1.3 m because the sampling line protrudes into the chamber over a distance of 0.5 m in order to sample air from the well-mixed center region of the chamber. Additionally, the sampling line has to bridge the thermal housing around the chamber walls.

At CLOUD, the stainless steel sampling lines have an inner diameter of 0.5" or 1" and 0.75 m total length (a 1" sampling probe was used for the water cluster CI-APi-TOF, where the instrument has a sampling line of 0.55m total length). The tips are located 0.35 m from the chamber walls to avoid sampling air from the boundary layer. Thus, after connecting to the CLOUD chamber, the total length of the sampling line of our instrument is 1.3m.

Line 443:

[…] the sample line penetration efficiency can be estimated as 33.7% for a laminar flow […]

[…] the sample line penetration efficiency is estimated to be 33.7% for a laminar flow […]

Line 445-446:

[…] the sampling line not always acts as a perfect sink for ammonia due to desorption and re-evaporation.

[…] the sampling line does not always act as a perfect sink for ammonia, due to partial re-evaporation.

Line 446-447:

[…] Furthermore, the interactions of ammonia with the surface of the sampling line depend on the humidity.

[…] Furthermore, the interactions of ammonia with the inner walls of the sampling line depend on the humidity of the sampled air.

Line 452-453:

significantly smaller and decreases to ~5×10^{12} cm^{-2} for a water vapor mixing ratio of 3500 ppmv at 278 K, which can be explained by the displacement of ammonia by water molecules (Vaittinen et al., 2014).

We mentioned this explanation in a sentence before (same Section), where we also cited Vaittinen et al. Thus, we decided to change this sentence to:

significantly smaller and decreases to ~5×10^{12} cm^{-2} for a water vapor mixing ratio of 3500 ppmv at 278 K.

Line 453-455:

This indicates that, depending on the ammonia mixing ratio and the gas conditions (temperature and RH), eventually an equilibrium can be reached between the gas and the surface. In such a case, no wall loss correction would be necessary.

Eventually an equilibrium is reached between the condensation on and evaporation from the walls, depending on the ammonia mixing ratio, RH and temperature. At equilibrium, ammonia losses from the chamber are due to dilution alone, and ammonia losses in the sampling line are negligible.

Line 456:

[…] if saturation happened at higher concentrations previously.

[…] if saturation happened previously at higher concentrations.

Line 461-463:

We are aware that the sampling line losses introduce some uncertainty on the ammonia measurement. However, this is an effect other in-situ techniques also have to struggle with (see, e.g., Leifer et al. (2017)).

Sampling line losses introduces up to a factor 3 uncertainty in the ammonia measurement, corresponding to transmission efficiencies between 33.7% and 100% for walls that are a perfect sink and zero sink, respectively. Variable sampling efficiency is a general problem facing most ammonia measurements (e.g., Leifer et al. (2017)).

Line 463:

We also want to note that the effect is much smaller for larger molecules, e.g. the penetration […]

The uncertainty is smaller for larger molecules, e.g. the sampling efficiency […]

Line 469-471:

As mentioned in Section 3.5 and shown in Table 1, the same calibration factor derived for ammonia was used to estimate the mixing ratio of dimethylamine. We caution, that this assumption can lead to uncertainties as the sensitivity of the measurement is expected to depend on the proton affinity of the measured substance (Hanson et al., 2011).

The same calibration factor as derived for ammonia was used to determine the mixing ratio of dimethylamine (Section 3.5 and Table 1). This assumption can lead to uncertainties as the sensitivity of the instrument is expected to depend on the proton affinity of the measured compound (Hanson et al., 2011).

Line 472:

[…]measured with the water cluster CI-APi-TOF […]

[…] measured by the water cluster CI-APi-TOF […]

Line 476-477:

The dilution life time during CLOUD13 is 6000 s and represents the maximum possible life time when wall loss would be negligible.

The chamber dilution lifetime represents the maximum possible lifetime when wall loss would be negligible (Section 3.7).

Line 478-479:

Figure 9a shows the time period when dimethylamine was added.

Figure 9a shows a period when dimethylamine was added to the chamber.

Line 482:

[…] estimated mixing ratios are generally in good agreement with each other when the wall loss life time is used to estimate the mixing ratios.

[…] estimated mixing ratios are generally in good agreement with each other.

Line 482-483:

Fluctuations in the measured mixing ratio can be explained by changes in the fan speed.

The response to changes of fan speed is initially sharp but gradually weakens as the walls progessively adsorb more dimethylamine.

Line 492-494:

Figure 9b shows a measurement of the chamber background for dimethylamine carried out during CLOUD13 over a time period of 5 days. The mean instrumental background for the time period shown in Figure 9b is ~0.14 pptv (for a temperature of 278 to 290 K and a relative humidity between ~50 and 60 %). The background values shown here are close to the background values obtained for 80% RH and 278 K (see Table 1).

Figure 9b shows a measurement of the background dimethylamine in the chamber, measured over 5 days during CLOUD13. The mean background is 0.14 pptv at 50-60% RH and temperatures of 278-290 K. These are similar to the backgrounds measured at 80% RH and 278 K (Table 1).

Line 497-498:

The estimated detection limits shown here are below or at similar detection limits reported in previous publications (You et al., 2014; Simon et al., 2016).

The estimated detection limits shown here are below or at similar levels compared to those reported in previous publications (You et al., 2014; Simon et al., 2016).

Line 501:

[…] experiments for ammonia, dimethylamine and iodic acid measurements.

[…] experiments to measure ammonia, dimethylamine and iodic acid.

Line 501-502:

During the experiments involving iodide, neutral clusters containing up to 4 iodine atoms are detected.

During experiments involving iodide, neutral clusters containing up to 4 iodine atoms were detected.

Line 502-503:

The technique has unprecedented low detection limits regarding the ammonia measurement as well as a fast time response and time resolution.

The instrument has demonstrated unrivalled low detection limits for ammonia, as well as a fast time response and time resolution.

Line 503-505:

A next step is its application to atmospheric measurements. The technique should be suitable for such measurements as the amount of clean gas required (ca. 2 slm of argon and some oxygen) is rather small and can easily be supplied with gas bottles (one argon gas bottle, 50 liters at 200 bar should last ~3 days).

We believe this instrument can readily be applied to atmospheric measurement. The amount of clean gas required for the corona tip (2 slm of argon and some oxygen) is rather small and can easily be supplied with gas bottles (one argon gas bottle of 50 liters at 200 bar should last about 3 days).

Line 506:

[…]can be taken from the chamber.

[…]can be drawn from the chamber.

Line 510-511:

[…]further signals corresponding to NH_4^+, NDH_3+, $ND_2H_2^+$ were also visible in the spectra due to deuterium-hydrogen exchange, which makes this method unfavorable.

[…]further signals corresponding to NH_4^+, NDH_3+, $ND_2H_2^+$ were also present due to deuterium-hydrogen exchange, which makes this method unsuitable.

Line 511-512:

[…] is also unfavorable since […] even with a high resolution mass spectrometer.

[…] is also unsuitable since the […] even for a high resolution mass spectrometer.

Line 514:

[…] which leads to greatly reduced sampling line losses and improved time response during ammonia measurements.

[…] which reduces sampling line losses and sharpens the time response for ammonia measurements.

Line 516-517:

We also tested the passivation technique, however, the […]

We tested this passivation technique but found it unsuitable for our instrument; the […]

Line 518:

[…]led to a consumption of the reagent ions since […]

[…] led to excessive consumption of the reagent ions since […]

Line 523-525:

The set-up and characterization of a water cluster Chemical Ionization-Atmospheric Pressure interface-Time Of Flight mass spectrometer (CI-APi-TOF) is described.

We have described the design and performance of a novel water cluster Chemical Ionization-Atmospheric Pressure interface-Time Of Flight mass spectrometer (CI-APi-TOF) for measurements of ammonia, amines (dimethylamine) and iodine compounds.

Line 525-526:

The generated protonated water clusters ($(H_2O)_{n\geq1}H_3O^+$) are used to selectively ionize compounds […]

The protonated water clusters ($(H_2O)_{n\geq1}H_3O^+$) selectively ionize compounds […]

Line 528-529:

The water cluster CI-APi-TOF was used at the CLOUD chamber where very low background ammonia mixing ratios (ca. 4 pptv at 278 K) were achieved.

The water cluster CI-APi-TOF was operated at the CLOUD chamber where very low background ammonia mixing ratios were measured (4 pptv at 278 K).

Line 529-530:

The level of detection (LOD) was estimated as 0.5 pptv for NH_3. To our knowledge, such a low detection limit for ammonia measurements has not been reported so far.

The limit of detection (LOD) for ammonia was estimated as 0.5 pptv. To our knowledge, such a low detection limit for ammonia measurements is unprecedented.

Line 532:

[…] was observed when using nitrogen instead of argon.

[…]was observed when nitrogen was used instead of argon.

Line 532-534:

Although, the sensitivity towards the measurement of NH_3 depends somewhat on the relative humidity of the sample flow, the observed sensitivity changes were rather low and can be taken into account by a correction factor.

The instrument shows some sensitivity to relative humidity of the sample flow (factor 3 increase in signal from 5% to 80% RH). However, this can be readily measured and corrected.

Line 537:

[…] iodine species. A total of 29 different iodine-containing compounds were unambiguously identified […]

[…] iodine compounds. A total of 29 different iodine-containing compounds were identified […]

Line 539:

[…] measuring iodic acid during CLOUD.

[…] measuring iodic acid.

Line 541:

[…] for which the nitrate CI-APi-TOF is calibrated for.

[…] for which the nitrate CI-APi-TOF was calibrated for.

Line 541-542:

The estimated LOD for the water cluster CI-APi-TOF regarding iodic acid was as low as 0.007 pptv.

In this way, we estimated the LOD for iodic acid in the water cluster CI-APi-TOF to be 0.007 pptv.

Line 544-545: We added the following sentence:

Laborarory and ambient measurements indicate increased importance of ammonia for new particle formation and growth in both pristine and polluted environments.

Line 547-548:

Airborne measurements in the upper troposphere, where very low ammonia mixing ratios can be expected (Höpfner et al., 2016) should in principle be feasible as well. For such measurement the water cluster CI-APi-TOF technique should be very well-suited due to the very low LODs that can be realized.

The water cluster CI-APi-TOF technique is also well-suited for airborne measurements in the upper troposphere, where fast response times and low detection limits are vital (Höpfner et al., 2016).

List of relevant changes made in the manuscript

- We revised our Section 3.3 (“response times”). We updated the xlabel of our Figure 4 towards seconds (s) in order to be consistent with the text, where we give response times in seconds. Next to this, we changed our description in Section 3.3, where we now distinguish between “instrumental response time” and “line response time” in a more clear way. We also state, which response times are shown in our figure 4.
- We revised our Section 3.7 (“CLOUD chamber characterization”), where we now state the detection limit of the PICARRO in the beginning of the discussion. Next to this, the discussion related to response times at low ammonia concentrations has been updated accordingly.
- We made minor corrections to our figures 1, 6 and 7 to improve clarity and to stay more consitent with our text.
- We have made several minor text corrections throughout the manuscript to improve legibility.
- To stay consistent with the text, where we mainly use “iodine compounds”, we changed the title of our manuscript from “*Measurement of ammonia, amines and iodine species using protonated water cluster chemical ionization time of flight mass spectrometry”* to “*Measurement of ammonia, amines and iodine compounds using protonated water cluster chemical ionization time of flight mass spectrometry”*

Measurement of ammonia, amines and iodine compounds using protonated water cluster chemical ionization mass spectrometry

Joschka Pfeifer[1,2], Mario Simon[2], Martin Heinritzi[2], Felix Piel[2,a], Lena Weitz[2,b], Dongyu Wang[3], Manuel Granzin[2], Tatjana Müller[2], Steffen Bräkling[4], Jasper Kirkby[1,2], Joachim Curtius[2], and Andreas Kürten[2]

[1]CERN, Geneva, 1211, Switzerland
[2]Institute for Atmospheric and Environmental Sciences, Frankfurt Am Main, 60438, Germany
[3]Paul Scherrer Institute, Villigen, 5232, Switzerland
[4]TOFWERK AG, Thun, 3600, Switzerland

[a]now at: Ionicon Analytik GmbH, 6020 Innsbruck, Austria
[b]now at: GSI Helmholtzzentrum für Schwerionenforschung GmbH, Darmstadt, 64291, Germany

Correspondence to: Joschka Pfeifer (joschka.pfeifer@cern.ch)

Abstract. Here we describe the design and performance of a new water cluster Chemical Ionization-Atmospheric Pressure interface-Time Of Flight mass spectrometer (CI-APi-TOF). The instrument selectively measures trace gases with high proton affinity such as ammonia and dimethylamine, which are important for atmospheric new particle formation and growth. Following the instrument description and characterization, we demonstrate successful measurements at the CERN CLOUD (Cosmics Leaving OUtdoor Droplets) chamber where very low ammonia background levels of ~4 pptv were achieved (at 278 K and 80% RH). The limit of detection of the water cluster CI-APi-TOF is estimated to be ~0.5 pptv for ammonia. Although no direct calibration was performed for dimethylamine (DMA), we estimate its detection limit is at least 3 times lower. Due to the short ion-molecule reaction time and high reagent ion concentrations, ammonia mixing ratios up to at least 10 ppbv can be measured with the instrument without significant reagent ion depletion. Besides the possibility to measure compounds like ammonia and amines (dimethylamine), we demonstrate that the ionization scheme is also suitable for the measurement of trace gases containing iodine. During CLOUD experiments to investigate the formation of new particles from I_2, many different iodine-containing species were identified with the water cluster CI-APi-TOF. The compounds included iodic acid as well as neutral molecular clusters containing up to four iodine atoms. However, the molecular structures of the iodine-containing clusters are ambiguous, due to the presence of an unknown number of water molecules. The quantification of iodic acid (HIO_3) mixing ratios is performed from an inter-comparison with a nitrate CI-APi-TOF. Using this method the detection limit for HIO_3 can be estimated as 0.007 pptv. In addition to presenting our measurements obtained at the CLOUD chamber, we discuss the applicability of the water cluster Ci-APi-TOF for atmospheric measurements.

1 Introduction

Ammonia (NH_3) is an important atmospheric trace gas that is mainly emitted by agricultural activity due to animal husbandry, use of fertilizers, and by vehicles in urban environments. It can partition to the aerosol phase and is one of the most important compounds contributing to secondary aerosol formation (Jimenez et al., 2009). Strong reductions in $PM_{2.5}$ mass and the associated adverse health effects could potentially be achieved by decreasing ammonia emissions (Pozzer et al., 2017). However, ammonia is not only partitioning to existing particles, but is also a key vapour driving new particle formation due to its stabilization of newly-formed clusters in ternary (sulfuric acid-water-ammonia) and multi-component (sulfuric acid-water-ammonia-highly oxygenated organic molecules) systems (Kirkby et al., 2011; Kürten et al., 2016a; Lehtipalo et al., 2018). On a global scale, a large fraction of newly formed particles and cloud condensation nuclei involves ammonia (Dunne et al., 2016). The involvement of ammonia in nucleation has recently been measured in the free troposphere, in Antarctica, and in the boreal forest (Bianchi et al., 2016; Jokinen et al., 2018; Yan et al., 2018). In the upper troposphere, model calculations suggest that ammonia is important for new particle formation and early growth (Dunne et al., 2016). Recent satellite measurements support this finding by the observation of up to several tens of pptv (parts per trillion by volume) of ammonia over Asia (Höpfner et al., 2016). Ammonia has a very strong effect on nucleation involving sulfuric acid and water, e. g., recent studies have shown that very low amounts of NH_3 in the pptv-range, or even below, can enhance nucleation rates by orders of magnitude compared with the pure binary system of sulfuric acid and water (Kirkby et al., 2011; Kürten et al., 2016a; Kürten, 2019). Stronger basic compounds like amines or diamines, have been shown to enhance nucleation rates, despite their much lower atmospheric concentrations (Almeida et al., 2013; Kürten et al., 2014; Jen et al., 2016; Yao et al., 2016). The experimental measurements are confirmed by quantum chemical calculations that compare the stabilizing effects of ammonia, amines, and diamines (Kurtén et al., 2008; Elm et al., 2017; Yu et al., 2018). For these reasons improved gas-phase measurements of these compounds are required. Sensitive real-time measurements are needed spanning mixing ratios over a broad atmospheric range between a few pptv to a few ppbv of ammonia in the boundary layer, and around a few pptv of amines (Ge et al., 2011; Hanson et al., 2011; You et al., 2014; Kürten et al., 2016b; Yao et al., 2016).

In some previous studies, ammonia has been measured using optical absorption or chromatographic methods (Norman et al., 2009; Bobrutzki et al., 2010; Verriele et al., 2012; Bianchi et al., 2012; Pollack et al., 2019). These measurement techniques are often specialized for the detection of only a few selected compounds, whereas chemical ionization mass spectrometry (CIMS) can often measure a suite of atmospheric trace gases simultaneously at low concentrations and high time resolution. The use of different reagent ions has been described in the literature for ammonia and amine measurements, e. g., protonated acetone, protonated ethanol, O_2^+, and protonated water clusters have been successfully applied (Nowak et al., 2007; Norman et al., 2007; Benson et al., 2010; Hanson et al., 2011; You et al., 2014; Yao et al., 2016). Nowak et al. (2010) deployed their instrument on an aircraft for measurements at up to ~5 km altitude. The reported limits of detection (LOD) varies between 35 pptv (You et al., 2014) and 270 pptv (Norman et al., 2009) for ammonia, whereas dimethylamine (and other amines) can be detected in the sub-pptv range (You et al., 2014; Sipilä et al., 2015; Simon et al., 2016). In this study we introduce a newly

developed chemical ionization mass spectrometer that uses protonated water clusters for selective ionization of ammonia and dimethylamine. The instrument is a high resolution Chemical Ionization-Atmospheric Pressure interface-Time Of Flight mass spectrometer (CI-APi-TOF, Aerodyne Inc. and TOFWERK AG) combined with a home-built ion source. The instrument is called a water cluster CI-APi-TOF, naming it in accordance with other established techniques using the same mass spectrometer but different reagent ions, e.g., the nitrate CI-APi-TOF for sulfuric acid, highly-oxygenated organic molecule, and cluster measurements (Jokinen et al., 2012; Ehn et al., 2014; Kürten et al., 2014). Here we describe and characterize the instrument during experiments performed at the CLOUD (Cosmics Leaving OUtdoor Droplets) chamber at CERN (European Organization for Nuclear Research). We show that the ammonia LOD is below 1 pptv, which is unprecedented to our knowledge. Besides measurement of basic compounds with high proton affinity, we find that the protonated water clusters are also well-suited to measure iodine-containing species such as iodic acid (HIO_3) and neutral molecular clusters containing up to four iodine atoms. The corresponding signals in the mass spectra were identified during CLOUD experiments on new particle formation from oxidation of iodine vapour. The relevance of such compounds for nucleation in the atmosphere has recently been reported (Sipilä et al., 2016). Our findings indicate that the water cluster CI-APi-TOF can provide sensitive real-time measurements of several trace gases that are important for atmospheric new particle formation and growth: ammonia, amines (dimethylamine) and iodine species.

2. Methods

2.1 CLOUD chamber

The measurements presented here were carried out at the CLOUD (Cosmics Leaving OUtdoor Droplets) chamber at CERN (European Organization for Nuclear Research) during fall 2017 (CLOUD12 campaign) and fall 2018 (CLOUD13). The CLOUD chamber is used to investigate new particle formation from different trace gas mixtures under controlled atmospheric conditions of temperature, relative humidity, UV light intensity and ionization (Kirkby et al., 2011; Kupc et al., 2011; Duplissy et al., 2016). The cylindrical stainless steel chamber has a volume of 26.1 m^3. It is designed to ensure that trace gas contaminants are low enough to allow precisely controlled nucleation experiments (Kirkby et al., 2016). The chamber is continuously flushed with synthetic air generated from liquid nitrogen and oxygen. The temperature and relative humidity of the air inside the chamber can be precisely controlled. For the present study, ammonia and dimethylamine from gas bottles were injected by a two-step dilution system (Simon et al., 2016; Kürten et al., 2016a). The calibration of the water cluster CI-APi-TOF with ammonia (Figure 1) was carried out while the instrument was disconnected from the chamber. For the calibration measurements, the two-step dilution system from the CLOUD chamber was replicated (Figure 1 and Section 2.2).

Iodine is introduced into the chamber by nitrogen flowing over solid, molecular iodine (I_2, Sigma-Aldrich, 99.999% purity) placed in a stainless steel evaporator immersed in a water bath at 303 K, with a temperature stability near 0.01 K. The generation of iodine-containing species for new particle formation is initiated by photolysis of I_2 in the CLOUD chamber in

presence of ozone and water. Measurements presented here were carried out at chamber temperatures between 223 and 298 K, with relative humidity (RH) ranging between 10 and 90%. A Pt100 sensor string measured the air temperature in the CLOUD chamber (Dias et al., 2017).

A chilled dew point mirror (Edgetech Instruments) measured the dew point inside the CLOUD chamber. The relative humidity is derived from water vapour pressure formulations published by Murphy and Koop (2005). Additionally, the RH was measured by a Tunable Diode Laser system (TDL) developed by Karlsruhe Institute for Technology (KIT), which was installed in the mid plane of the chamber (Skrotzki, 2012). The relative humidity was derived using the mean value of both instruments, with a combined measurement uncertainty of 5%.

2.2 Water cluster CI-APi-TOF

The selective detection of ammonia and amines by atmospheric pressure chemical ionization using positively-charged water clusters has been demonstrated previously (Hanson et al., 2011). The same ionization technique is used in the present study. The reagent and product ions are measured with an Atmospheric Pressure interface-Time Of Flight mass spectrometer (APi-TOF), which is coupled with a newly-designed crossflow chemical ionization (CI) source operated at ambient pressure (Figure 1). The reagent ions, i.e., protonated water clusters ($(H_2O)_nH_3O^+$) are generated by positive corona discharge in the presence of argon (95 %), oxygen (5 %), and water vapor. The water vapor is added by bubbling the argon through a stainless steel humidifier (containing about 1 liter of Millipore purified water) held at ambient temperature of near 20 °C. As suggested by Hanson et al. (2011), a few droplets of sulfuric acid were added to the water in order to minimize potential contamination with ammonia from the water supply. Flow rates of 2.5 standard liters per minute (slm) for argon and 0.1 slm for oxygen were used. All flow rates were controlled by calibrated mass flow controllers (MFC). A conversion factor for the measured argon flow (provided by the MFC manufacturer) was applied. Initially we used nitrogen instead of argon for the flow that passes the corona needle, but this resulted in much higher ammonia backgrounds. This is likely due to NH_3 production in the corona plasma when nitrogen is present (Haruyama et al., 2016). Furthermore, the addition of oxygen is necessary for the generation of a stable corona discharge in positive mode when using argon as the main ion source gas (Weissler, 1943).

Protonated water is also used in proton-transfer-reaction mass spectrometry (PTR-MS) that has been described in numerous publications (Good et al., 1970; Kebarle, 1972; Zhao and Zhang, 2004; Hansel et al., 2018). A simplified reaction scheme leading to the formation of protonated water clusters is shown as follows (Sunner et al., 1988):

$$e^- + O_2 \rightarrow O_2^+ + 2\,e^-, \quad \text{(R1)}$$

$$O_2^+ + (H_2O)_2 \rightarrow O_2^+(H_2O)_2 \rightarrow H_3O^+(OH) + O_2, \quad \text{(R2)}$$

$$H_3O^+(OH) + (H_2O)_n \rightarrow H_3O^+(H_2O)_n + OH. \quad \text{(R3)}$$

The PTR-MS operates its ion-molecule reaction zone (IMR) typically at low pressure (~ 10 hPa) and uses an electric field (~ 100 V mm^{-1}) to break up water clusters so that mainly non-hydrated H_3O^+ ions remain. The use of charged water clusters ($(H_2O)_{n\geq1}H_3O^+$ instead of H_3O^+) can increase the selectivity as water clusters have a much higher proton affinity compared with the water monomer (Aljawhary et al., 2013). However, due to their high proton affinity, ammonia and amines can still be detected according to the following reaction scheme:

$$H_3O^+(H_2O)_n + \mathrm{X} \rightarrow \mathrm{X}H^+(H_2O)_b + (n+1-b)\cdot(H_2O), \qquad \text{(R4)}$$

where X represents the target substance that is ionized in the ion-molecule reaction zone (see below) and detected in the mass spectrometer. Since water molecules can evaporate in the atmospheric pressure interface of the mass spectrometer, some of the product ions are detected without water, e. g., ammonia is mainly detected as NH_4^+ (see Figure 2).

A schematic drawing of the calibration setup and the ion source is shown in Figure 1. The gas mixture for the ion source is composed of argon, oxygen and water vapor. It is introduced from two lines placed in the opposite direction to each other at an overall flow rate of ~2.6 slm (Figure 1a). The electrodes of the ion source are displayed in red colors in Figure 1b. The connection to the mass spectrometer is shown using blue color. The 1" sampling line and the inlet (22 mm inner diameter) consist of stainless steel and are shown in green color. Components used for insulation are shown in white colors. A total sample flow rate of ~ 19.5 slm is maintained by a vacuum pump and a mass flow controller. The overall length of the sampling line connecting the CLOUD chamber and the ion molecule reaction zone is 1.3 m. A voltage of 3600 V is applied to the corona needle while 500 V are applied to the conically-shaped counter electrode (Electrode 1 in Figure 1b) made of stainless steel. The housing of the ion source is made of polyether ether ketone (PEEK). The ion source gas and the generated reagent ions flow through a funnel (smallest inner diameter 2.5 mm) before they mix with the sample flow. A small capillary (inner diameter of 0.8 mm) is located opposite of the funnel (Electrode 2 in Figure 1b). The electric field between the counter electrode and the capillary (at ground potential) accelerates the ions towards the entrance of the mass spectrometer. The pinhole plate (pinhole inner diameter of 350 µm) and the capillary are in electric contact and ~0.8 slm flow through the capillary and the pinhole into the mass spectrometer. The measured product ions are generated in the ion-molecule reaction zone (IMR, yellow area in Figure 1a) at atmospheric pressure. The dimension of the IMR is defined by the distance between the counter electrode and the capillary (~ 16.4 mm). After passing the pinhole, the ions are transported through two quadrupoles (Small Segmented Quadrupole, SSQ and Big Segmented Quadrupole, BSQ) towards the detection region of the mass spectrometer (Micro-Channel Plate, MCP; pressure is approx. 1×10^{-6} hPa). The estimated reaction time is <1 ms. This short reaction time allows the measurement of high ammonia mixing ratios (up to ~10 ppbv) without significant depletion of the reagent ions, which would be the case when using an ion source design for the measurement of sulfuric acid (Eisele and Tanner, 1993; Kürten et al., 2011), which is typically present at much lower concentrations than ammonia. The principle of a cross-flow ion source was introduced by Eisele and Hanson (2000) who used this technique to detect molecular sulfuric acid clusters. In more recent

studies, this technique was used for the measurement of ammonia (Nowak et al., 2002; Nowak et al., 2006; Hanson et al., 2011).

The measured volume mixing ratio (VMR, in pptv) of detected compounds is derived from a calibration factor (*C*) and the sum of the product ion counts per second (pcs) normalized against the sum of the reagent ion counts per second (rcs) (Kürten et al., 2016b; Simon et al., 2016):

$$VMR = C \cdot \ln\left(1 + \frac{\sum pcs}{\sum rcs}\right) = C \cdot ncps. \quad (1)$$

Equation (1) yields the VMR measured by the water cluster CI-APi-TOF as a function of the normalized counts per second (*ncps*). A calibration factor, *C*, which includes factors like the reaction rate and the effective reaction time, is required to convert the *ncps* to a mixing ratio. This factor can be derived from the inverse slope of a calibration curve (see Section 3.2). While Hanson et al. (2011) report a maximum for the water cluster distribution at the pentamer, evaporation of water seems to be stronger in our instrument. The maximum signal in clean spectra is usually found for the water dimer ($(H_2O)H_3O^+$, see Figure 2) and a strong drop in the reagent ion signals is found beyond the tetramer ($(H_2O)_3H_3O^+$). Therefore, the sample quantification includes, using ammonia as an example, the product ions $(H_2O)_nNH_4^+$ with n = 0,1 and the reagent ions $(H_2O)_mH_3O^+$ with m = 0-3. Possible losses in the sampling line are not taken into account by the calibration factor (see Section 3.8 for discussion of sampling line losses). The only compound for which a direct calibration is performed in the present study is ammonia (Section 2.3). When mixing ratios for dimethylamine are presented, the same calibration factor is used. This approach can introduce uncertainty as the proton affinity, as well as transmission efficiency differ for dimethylamine compared to ammonia. However, previous studies showed that the ionization efficiency from protonated water clusters is collision-limited for both compounds, ammonia and dimethylamine (Sunner et al., 1988; Hanson et al., 2011). The applicability of this approach is discussed in Section 3.9; it is estimated that the mixing ratios for dimethylamine are correct within a factor of ~3.5.

2.3 Calibrations

2.3.1 Ammonia

During calibrations, ammonia was drawn from a gas bottle containing an NH_3 mixing ratio, *B*, of 100 ppmv diluted in pure nitrogen (Air Liquide, ±5% uncertainty for the certified NH_3 mixing ratio). It was diluted in two steps, where MFCs (shown as M_n in Figure 1a) are used to obtain different set points for the volume mixing ratio (Figure 1a). During the second dilution step the mixture from the first dilution is injected into the center of the main sample flow (flow rate, Q_{sample}). The theoretical VMR_{theor} is given by (Simon et al., 2016):

$$VMR_{theor} = \frac{M_1}{M_1+M_2} \cdot \frac{M_3}{M_3+Q_{sample}} \cdot B. \quad (2)$$

The flow of ammonia from the gas bottle is set by M_1 (0.01 slm max.), whereas M_2 (2 slm range) controls the flow of nitrogen for the first dilution step. The flow of diluted ammonia that is introduced into the sample flow is controlled by M_3 (0.1 slm range). The calibration flow consists of the same synthetic air as used for the CLOUD chamber. The flow is provided by two MFCs that control a dry portion (M_4) and a wet portion of the flow that has passed a stainless steel water bubbler (M_5, see Figure 1). By adjusting M_4 and M_5 (both 50 slm range) the RH of the sample flow can be controlled in order to test whether a humidity dependence exists for reaction (R4). Care is taken that the sum of M_4 and M_5 is always somewhat larger than Q_{sample}. To avoid overpressure in the sampling line, the excess flow is vented through an exhaust before the sampling line.

Accordingly, the measured sample air consists of synthetic air (80% nitrogen, 20% oxygen) with adjustable RH and ammonia mixing ratio. Results of the calibrations are discussed in Section 3.2.

2.3.2 Iodine Oxides

The water cluster chemical ionizer is also effective for iodine-containing species, which were detected in new particle formation experiments from I_2 photolysis during CLOUD13. Prominent signals of iodic acid ($HIO_3 \cdot H^+$ and $HIO_3 \cdot H_3O^+$) were observed among many iodine compounds (Section 3.6 and Table 2). These species can be unambiguously identified due to the large negative mass defect of the iodine atom and the high resolution (> 3000 Th/Th) of the mass spectrometer. No direct calibration for HIO_3 was performed; however, a second chemical ionization mass spectrometer at CLOUD, using nitrate reagent ions (nitrate CI-APi-TOF), was also measuring HIO_3 simultaneously. Therefore, a calibration factor for HIO_3 has been derived by scaling concentrations measured by the nitrate CI-APi-TOF, which itself had been calibrated for sulfuric acid (Kürten et al., 2012). We further assume that both sulfuric and iodic acid are detected with the same efficiency by the nitrate CI-APi-TOF. This assumption introduces uncertainty when estimating the detection limit of HIO_3. However, as the reaction of sulfuric acid with nitrate ions is at the kinetic limit (Viggiano et al., 1997), the detection limits shown here based on this assumption can be seen as lower limits. Unfortunately, there is currently no direct calibration technique established for iodic acid in the gas phase. The assumption we use in the present study was also applied in a previous study for deriving gas phase concentrations of iodic acid (Sipilä et al., 2016).

For the instrument inter-comparison (and the indirect calibration of the water cluster CI-APi-TOF), 18 different CLOUD experimental runs were selected and mean values were calculated for different steady-state concentrations. We took 6 steady-state concentrations each at temperatures of 263 K (80% RH) and 283 K (40% RH and 80% RH).

2.4 PICARRO

A PICARRO G1103-t NH_3 Analyzer (PICARRO Inc., USA) measuring ammonia mixing ratios based on cavity-ring down spectroscopy was also connected to the CLOUD chamber during CLOUD12 and CLOUD13. The instrument is suitable for real-time monitoring of ammonia in ambient air and has been presented in previous studies (Bell et al., 2009). The G1103-t was installed at the CLOUD chamber with its own sampling line coated with Sulfinert (Restek GmbH, Germany), where the coating reduced the losses of ammonia to the sampling line walls considerably. Since the PICARRO has a rather small sample

flow rate (<1 slm), an additional pump was used to enhance the flow rate to 5 slm just before the instrument inlet. This was done in order to minimize line losses and to shorten the response times. It was, however, not quantitatively tested in how far these measures (Sulfinert and increased flow rate) helped with the measurements. The PICARRO was also independently calibrated with a NH_3 permeation tube (Fine Metrology, Italy) using a multigas calibrator (SONIMIX 6000 C1, LNI Swissgas, Switzerland). The time interval for one measurement of the PICARRO is 5 seconds for which a lower detection limit of 200 pptv is specified (PICARRO Inc., USA; Martin et al., 2016). By using the same method (at the same time period) as for the water cluster CI-APi-TOF (see Section 3.5), we derive a detection limit of 366.2 pptv for the PICARRO unit used in our study during CLOUD13. The detection limit derived for the PICARRO used during the CLOUD12 experiments is at 170.1 pptv.

3. Results and Discussion

3.1 Main peaks in spectrum

Figure 2 shows a typical spectrum during calibrations, where 10 ppbv of ammonia are injected (40% RH, ~293 K). The most prominent primary ions are H_3O^+, $(H_2O)H_3O^+$ and $(H_2O)_2H_3O^+$. The dominant primary ion is $(H_2O)H_3O^+$. The water tetramer ($(H_2O)_3H_3O^+$) is usually the largest water cluster that can be detected. The addition of ammonia generates NH_4^+ and $(H_2O)NH_4^+$; a small signal from NH_3^+ is also visible. At low ammonia concentrations the signal from NH_4^+ has a similar magnitude as H_2O^+ (which may arise from reactions of O_2^+ and H_2O). Since these ions have the same integer mass, a high mass resolving power is essential to reach low detection limits for ammonia as otherwise the differentiation between the two signals is not possible. At low mass, the APi-TOF used in the present study has a resolving power of ~2000 Th/Th, which is sufficient to separate the two peaks. For the analysis of the spectra, the software TOFWARE is used that allows analyzing high resolution spectra (Stark et al., 2015; Cubison and Jimenez, 2015; Timonen et al., 2016). Prominent peaks from N_2H^+, NO^+ and O_2^+ are also seen (Figure 2). It is not clear how these ions are formed and why they survive the relatively long reaction time of ~1 ms since Good et al. (1970) report that O_2^+ reacts rapidly away in moist air. For the analysis the presence of these background peaks is currently ignored and they are not counted as reagent ions (in equation 1) as we have no indication that they interact with the target species relevant for the present study. An exception could be NH_3^+ (possibly from reaction of O_2^+ and NH_3); however NH_3^+ is not considered and is only a small fraction of NH_4^+.

In contrast to the spectrum shown in Figure 2 with relatively small water clusters, Hanson et al. (2011) observe the highest signal in the water cluster distribution for the pentamer. We explain this difference in more pronounced fragmentation and evaporation of ion clusters in the atmospheric pressure interface of our mass spectrometer.

For estimating an ammonia mixing ratio (Equation 1), the product ion count rates are normalized to the dominating reagent ion count rates. Figure 2 shows that even at 10 ppbv ammonia the reagent ion signals are an order of magnitude higher than the product ion count rates. This indicates that very little reagent ion depletion occurs and thus the normalized counts per second are linear with the ammonia VMR at least up to 10 ppbv (see Section 3.2).

3.2 Ammonia and iodic acid calibration

Figure 3 shows the calibration curves obtained for NH_3 and HIO_3 during the CLOUD13 campaign. Each dot represents the mean value of a steady state measurement of at least 20 minutes. The normalized counts per second are based on the two highest signals assigned to the analyzed compound (NH_4^+ and $(H_2O)NH_4^+$ for ammonia and HIO_3H^+ and $HIO_3H_3O^+$ for iodic acid). The total error of the mixing ratios (*x*-axis) is calculated by Gaussian error propagation taking into account the standard deviation of the flow rates from the mass flow controllers and the uncertainty of the ammonia gas bottle concentration. Since we obtained the mixing ratio shown in Figure 3b by scaling the concentrations measured by a nitrate CI-APi-TOF calibrated for sulfuric acid, the error on the *x*-axis equals the uncertainty of these measurements (estimated as a factor of two for the iodic acid concentration). The error on the *y*-axis is given by the standard deviation of the normalized counts per second. We derive a calibration curve from a linear regression model using the Wilkinson-Rogers Notation (Wilkinson and Rogers, 1973). The fit is forced through the origin; however, even when the fit is not constrained, the resulting slope is essentially the same (the results for the slopes/sensitivities differ by 1.35%). The derived slopes represent the inverse of the calibration factor, *C* (~ 1.46×10^5 pptv at 40% RH), in equation (2). Figure 3 shows that all measured mixing ratios lie in the area of the confidence intervals (95% confidence intervals) and thus the linear model describes the dependency very well. The calibration was performed in September 2018, before the CLOUD13 campaign and also during and after the end of the campaign in December at relative humidities between ~3% and 82% and at ambient temperatures of the experimental hall near 293 K. The calibrations for ammonia were performed by introducing the highest mixing ratio first. However, it took almost a day to reach stable signals as the tubing and the two MFCs through which the ammonia was flown (M_1 and M_3) needed to equilibrate. The further calibration points were then recorded by reducing the flow rate of M_3. In this way, no change in the ammonia mixing ratio inside the capillary before the main sampling line and in the MFCs was necessary. This allowed for a relatively fast stepping through the calibration set points. However, even when the ammonia flow was shut-off there was still significant diffusion of ammonia from the capillary into the sampling line, which resulted in relatively high background values (with nominally zero NH_3). We therefore derived the limit of detection by measuring the ammonia background in the CLOUD chamber with the calibration lines disconnected from our instrument (Section 3.5). During the calibrations, the relative humidity was calculated by assuming that the sample flow passing the water reservoir is 100% saturated (Figure 1a). For the calibrations carried out after the campaign, the temperature of the total sample flow was measured to derive the absolute humidity. The calibration points in Figure 3 were taken at measured gas flow temperatures of 288 to 290 K. The relative humidity was set to 40% RH by adjusting the dry and the wet flow rates for the sample flow; these conditions correspond to an absolute humidity of ~ 0.0057 kg m^{-3}. The calibration factor derived for CLOUD12 (for ammonia) differs from the calibration factor shown here. This is due to a different ion source (designed for a 0.5'' sampling line in CLOUD12 compared with a 1'' line in CLOUD13), a different sample flow rate and different tuning of the CI-APi-TOF.

3.3 Response times

The response time of the water cluster CI-APi-TOF is defined as the characteristic time needed for the instrument to react on changes in the ammonia mixing ratio. We define the response time as the time required for the instrument to reach 95% of the new mixing ratio being injected. The response time takes into account two processes. It includes both the response time of the instrument ("instrumental response time") and the time for the lines to reach a steady state for ammonia delivery ("line response time"). Figure 4 indicates the typical response times of the water cluster CI-APi-TOF during calibrations (here at 60% relative humidity). It shows a decay between two calibration steps when the injected ammonia is reduced from 9509 pptv to 6911 pptv and a rise in the signal when the ammonia mixing ratio is increased from 500 pptv to 9509 pptv. Panel a) indicates a clear difference between the fast instrumental response time (red line) and slower line response time (black line). While we expect a similar behavior in instrumental response time for a decay from 9509 to 500 pptv, a longer line response time is expected due to re-evaporation of ammonia from the sampling lines. Thus, the mixing ratios were gradually reduced during calibrations. The instrumental response time shown in Figure 4 is at 6 s for a decay in mixing ratio (9509 pptv to 6911 pptv) and at 18 s for a rise (500 pptv to 9509 pptv). The line response time is at 37 s (decay) and at 890 s (rise). The experiments were repeated several times at varying relative humidities. The instrumental response time only varied by a few seconds during our experiments (between 6 to 10 s (decay) and 18 to 25 s (rise)). While the variation in instrumental response time is small, the line response time can vary strongly depending on precursor conditions and relative humidity. During our experiments, the line response time varied between 37 s and 54 s (decay) and between 535 s and 890 s (rise), respectively. Interactions of ammonia with the sampling line are discussed in Section 3.8.

3.4 Influence of the humidity on the sensitivity

Figure 5 shows the sensitivity of the ammonia measurements to relative humidity. These data are derived from calibration curves similar to that of Figure 3a. During the calibrations the humidity was changed by adjusting the dry and wet sample flow rates. For all conditions NH_4^+ has the highest product ion count rate. However, the ratio of the signals for $(H_2O)NH_4^+$ and NH_4^+ increases with humidity as well as the sensitivity. A possible explanation for the observed sensitivity dependence could be increased collision rates at high humidity where larger water clusters are present. In addition, the detection efficiency as function of the ion mass can vary depending on the voltages applied to the ion source and the APi-section, as well as the time of flight region of the mass spectrometer. Thus, the mass spectrometer does not have a constant detection efficiency over the full mass range (Heinritzi et al., 2016). A higher detection efficiency at *m*/*z* 36 ($(H_2O)NH_4^+$) compared with *m*/*z* 18 (NH_4^+) together with the higher fraction of $(H_2O)NH_4^+$ compared with NH_4^+ at high humidity could explain some of the observed effect. However, the observed increase in sensitivity is modest (increase by a factor of ~2.5 when the humidity increases by a factor of 10). Nevertheless, the effect is taken into account by using the measured relative humidity inside the CLOUD chamber (see Section 2.1) to correct the derived ammonia mixing ratio. The effect of temperature on the sensitivity could not be tested during a dedicated calibration experiment as our calibration setup was not temperature-controlled. However, during a transition

from 298 K to 248 K in the CLOUD chamber and constant ammonia injection, no significant change in the measured ammonia was observed, which indicates a weak influence of temperature.

For iodic acid measurements, the sensitivity to relative humidity and temperature is different (Figure 6). While NH_4^+, without any water molecule, is the dominant signal for ammonia, the highest iodic acid signal is $H_4IO_4^+$, which is $H_2O{\cdot}HIO_3H^+$ or $HIO_3{\cdot}H_3O^+$. We observed an increasing sensitivity at lower temperatures, while the humidity dependency appears to be smaller compared to the ammonia measurements (Figure 5). The higher counting rate of $H_4IO_4^+$ compared to $H_2IO_3^+$ indicates that iodic acid requires additional water in order to be associated with a positively charged ion. However, during the transition from ambient pressure into the vacuum of the mass spectrometer, water molecules can evaporate and leave $H_2IO_3^+$ in a non-equilibrium state. Besides the observation of iodic acid, additional signals from iodine-containing species can be found in the spectra. These compounds are listed in Table 2. Elucidating the exact formation pathways of these ions and the corresponding neutral species is a subject for future work.

3.5 Detection limits and instrumental backgrounds

Determining the limit of detection (LOD) for ammonia is complicated by changes in the observed background signal. During the calibrations a relatively high background was measured, which was decreasing slowly after the ammonia flow through the capillary was shut off. A typical value reached a couple of minutes after the ammonia flow was turned off is ~30-60 pptv. When the water cluster CI-APi-TOF was connected to the CLOUD chamber the NH_3 signals usually fell more rapidly when no ammonia was actively added. However, even under these conditions the ammonia was not zero and the measured signal changed when the RH or temperature of the chamber was adjusted, indicating the release of ammonia from the chamber walls. The ammonia contaminant level of the CLOUD chamber was previously determined to be several pptv at 278 K and 38% RH (Kürten et al., 2016a). During CLOUD13 the measured ammonia background was 3.7 pptv at 278 K and 80% RH, which confirms the previous estimate made with less sensitive ammonia instrumentation. The measured background also includes any contamination in the sampling line of the instrument. Another source of background ammonia could be the ion source. During the early stages of our development we used nitrogen instead of argon as the main ion source gas. This led to ammonia backgrounds of several 100 pptv since ammonia can be generated by the nitrogen plasma from the corona tip when it mixes with the humid sample flow (Haruyama et al., 2016). Replacing nitrogen with argon sharply decreased the background ammonia signals. Nevertheless, traces of nitrogen containing gases in the ion source could potentially contribute to the ammonia background. However, the ammonia background reduces at lower chamber temperatures, which argues against the ion source being a significant source of ammonia, since it is always at ambient temperature.

The LOD is defined as the additional ammonia mixing ratio that is necessary to exceed three standard deviations of the background fluctuations (You et al., 2014). This value corresponds to 0.5 pptv for an averaging time of 1 minute. Assuming the same sensitivity as for ammonia and taking into account the background signals for the exact masses, we can estimate LODs for other compounds. Besides the calculated values for ammonia, Table 1 lists the estimated backgrounds and LODs for dimethylamine and iodic acid. High resolution data are necessary to reach the LODs shown in Table 1 since several species

may share the same integer mass. For example, for dimethylamine (exact mass of protonated compound at 46.0651 Th) other species like NO_2^+ (45.9924 Th) or CH_4NO^+ (46.0287 Th) can interfere. For dimethylamine only the peak with the highest count rate is taken into account, since $(C_2H_7N)H_3O^+$ interferes with other compounds measured during the experiments, even with high resolution data. In principle, the omission of the larger product ions (with one additional water molecule) should lead to a different calibration constant. However, the effect is small since for the measured bases, the ion signals with associated water are smaller than the products without the water molecule. The goodness of the assumption of using the calibration constant for dimethylamine as that derived for ammonia is discussed in Section 3.9.

The instrumental background for NH_3 is higher than the estimated backgrounds for the other compounds shown in Table 1. Ammonia is ubiquitous and hard to remove completely by water purification systems, so it can be introduced into the CLOUD chamber via the air humidification system. Nevertheless, the detection limit derived for ammonia is well below the LOD reported for other measurement techniques and instruments (von Bobrutzki et al., 2010; You et al., 2014; Wang et al., 2015). However, the performance of the water cluster CI-APi-TOF during atmospheric measurements remains to be tested. The dimethylamine level in the CLOUD chamber is mostly below the estimated LOD.

The estimated LOD of iodic acid is well below that of ammonia and dimethylamine (Table 1). We might explain this when looking at signals that could possibly interfere with the measured compounds. All compounds shown in Table 1 have an integer mass, where other signals are also detected, e.g., H_2O^+ at the nominal mass of ammonia, or NO_2^+ at the nominal mass of dimethylamine. For the high masses of the iodine containing species with their strong negative mass defects these isobaric compounds are much less crucial. Additionally, iodic acid has a much lower vapor pressure compared with ammonia and is not emitted efficiently from surfaces at temperatures relevant for the present study. Therefore, much lower backgrounds can be expected even if the sampling line and the instrument were exposed to high concentrations before.

3.6 Iodine identified species during CLOUD13

The CI-APi-TOF measurements of HIO_3 with positive water cluster ionization show excellent correlation with negative nitrate ionization (Figure 3b). Furthermore, we were able to detect iodine-containing species at higher mass to charge ratios (e.g., iodine pentoxides) during several experiments. Figure 7 shows the detected iodine species when a high I_2 concentration (~50-100 pptv) was injected into the chamber (mean values over a duration of 120 minutes). The derived mean iodic acid mixing ratio is ~0.98 pptv according to the measurements of the water cluster CI-APi-TOF. During this experiment, we observed compounds containing up to 4 iodine atoms. The size of the circles in Figure 7 corresponds to the mean count rate of the signals on a logarithmic scale. For comparison, the intensities of the reagent ions are also shown. Table 2 lists the sum formulas of some identified iodine species.

During some experiments, an electric field of about 20 kV/m was applied to the chamber to remove ions and study purely neutral (i.e., uncharged) nucleation. Even during these experiments the same signals as shown in Figure 7 were present. This indicates that the water cluster CI-APi-TOF measures neutral compounds after ionizing them in the ion-molecule reaction zone. The present study only gives a short overview of the iodine signals measured with the water cluster CI-APi-TOF. Further

CLOUD publications will focus on the chemistry of the iodine-containing species and on their role in new particle formation processes.

3.7 CLOUD chamber characterization

The performance of the water cluster CI-APi-TOF during CLOUD12 experiments with ammonia is shown in Figure 8. We compare the derived mixing ratios with the measurements of the PICARRO. In addition, both can be compared with the range of ammonia mixing ratios expected from the MFC settings for ammonia injected into the CLOUD chamber, the chamber volume and the ammonia life time (see, e.g., Simon et al. (2016) and Kürten et al. (2016a) for the equations linking these quantities to the estimated CLOUD mixing ratios). While the injected ammonia can be determined to better than 20% from the MFC settings, the ammonia life time in the chamber can span a wide range. For a very clean chamber or at very low temperatures the chamber walls represent a perfect sink and the ammonia has a short life time. A wall loss life time of 100 s at 12% fan speed was previously reported by Kürten et al. (2016a). Measurements with sulfuric acid indicate a factor of 4 increase of the wall loss rate when the fan speed is changed from the nominal setting of 12% to 100%. Scaling these measurements to the ammonia measurements yields a wall loss life time of 25 s at 100% fan speed. On the other hand, once the walls have been exposed for sufficient time with ammonia they reach an equilibrium where condensation and evaporation rates are equal. Under these conditions, the ammonia lifetime is determined by the chamber dilution lifetime alone (6000 s), and so the NH_3 increases to higher equilibrium concentrations. Furthermore the walls can act as a source of ammonia due to re-evaporation of ammonia molecules attached to the surface. This effect can be significant when the concentrations previously injected into the chamber were higher than the current concentrations. Thus, the estimated range can vary by a factor of ~200 based on the chamber conditions. This wide range is indicated by the shaded areas in Figure 8 (light blue color).

Figure 8a shows the measurements of the water cluster CI-APi-TOF, the PICARRO, and the calculated values for ammonia. The PICARRO trace is shown for the time when the detection limit (170.1 pptv during CLOUD12) is exceeded. The signal measured by the water cluster CI-APi-TOF follows the injected ammonia almost instantaneously (first injection is on Oct. 23). The slower response time of the PICARRO can be explained by a combination of the longer sampling line (~1.8 m compared to 1.3 m for the water cluster CI-APi-TOF) and the lower flow rate (~ 1 slm with a core sampling of 5 slm compared with ~ 20 slm for the water cluster CI-APi-TOF). After the flow of ammonia is shut off, both the mass spectrometer and the PICARRO show almost identical values as the chamber progressively releases ammonia from the walls. Before the first ammonia injection it can also be seen that the water cluster CI-APi-TOF shows progressively lower background ammonia values. Whether this is due to a gradual cleaning of the chamber, the instrument or the sampling line is unclear. Figure 8a also indicates the influence of temperature on the level of contaminant ammonia level after ammonia had been injected into the chamber. When the chamber temperature falls from 298 K to 278 K (shortly before Oct. 31) the contaminant NH_3 decreases by around a factor of 5 due to the lower evaporation rate of ammonia from the chamber walls.

The influence of changing relative humidity can be seen in Figure 8 between 29.10. and 30.10. Part of the change is due to the response of the water cluster CI-APi-TOF (Section 3.4). A second contribution arises since water molecules can

displace adsorbed ammonia on surfaces (Vaittinen et al., 2014). This effect can be pronounced when the chamber walls have been conditioned with high ammonia concentrations. It is important to note that the instrument was characterized for humidity dependency during the following CLOUD13 campaign. While changes in sensitivity with relative humidity were taken into account during CLOUD13, this was not the case during CLOUD12. The observed increase in mixing ratios at this time is a combination of a change in sensitivity of the instrument and an increase in the gas phase concentration of ammonia due to re-evaporation from the walls of the CLOUD chamber. Here, the PICARRO trace can provide insight into the magnitude of both effects indicating that the re-evaporation from the chamber walls dominates over the change in sensitivity. In Figure 8 during the early part of 25.10 the PICARRO shows a steep increase of ammonia while the water cluster CI-APi-TOF saturates near 20 ppbv, due to depletion of the primary ions. It is important to note that other vapor concentrations were also high at this time, which contributed to the depletion of the primary ions. During CLOUD13, where an improved version of the ion source was used (Section 3.2), significant depletion of primary ions was only observed above 40 ppbv ammonia.

Figure 8b shows how the ammonia mixing ratios vary with the mixing fan speed in the CLOUD chamber. The fan speed was varied between 12% (default value) and 100%. Since the temperature during these experiments was low (248 K), the chamber walls act as a fairly efficient sink for ammonia. Therefore, the measured mixing ratios respond promptly to the changing fan speed indicating a change of almost a factor 4 in ammonia. Moreover the measurements coincide with the values calculated from the MFC settings, assuming wall loss life times of 100 s and 25 s at 12% and 100% fan speed, respectively. Due to its higher detection limit, the PICARRO is insensitive at these low mixing ratios (green line in Figure 8b).

3.8 Ammonia wall loss rates in the sampling line

The largest uncertainty in the ammonia measurement is related to the sampling line losses. At CLOUD, the stainless steel sampling lines have an inner diameter of 0.5" or 1" and 0.75 m total length (a 1" sampling probe was used for the water cluster CI-APi-TOF, where the instrument has a sampling line of 0.55 m total length). The tips are located 0.35 m from the chamber walls to avoid sampling air from the boundary layer. Thus, after connecting to the CLOUD chamber, the total length of the sampling line of our instrument is 1.3m. For an ammonia diffusivity of 0.1978 $cm^2\ s^{-1}$ (Massman, 1998) and a sample flow rate of 20 slm, the sample line penetration efficiency is estimated to be 33.7% for a laminar flow (Dunlop and Bignell, 1997; Baron and Willeke, 2001; Yokelson, 2003). This means, that if the walls of the sampling line act as a perfect sink, then the measured NH_3 mixing ratios would need to be corrected with a factor of ~3. However, it is quite likely that the sampling line does not always act as a perfect sink for ammonia due to partial re-evaporation. Furthermore, the interactions of ammonia with the inner walls of the sampling line depend on the humidity of the sampled air. Water on surfaces can affect the uptake or release of ammonia. Vaittinen et al. (2014) showed that increased humidity can displace ammonia from surfaces. Additionally, water on surfaces can allow weak acids and bases to dissociate into their conjugate compounds on the surface, thereby affecting the partitioning to the surface (Coluccia et al., 1987). Vaittinen et al. (2014) studied the adsorption of ammonia on various surfaces and found a value of 1.38×10^{14} molecule cm^{-2} for the surface coverage on stainless steel. For humid conditions this value is, however, significantly smaller and decreases to ~5×10^{12} cm^{-2} for a water vapor mixing ratio of

3500 ppmv at 278 K. Eventually an equilibrium is reached between the condensation on and evaporation from the walls, depending on the ammonia mixing ratio, RH and temperature. At equilibrium, ammonia losses from the chamber are due to dilution alone, and ammonia losses in the sampling line are negligible. Furthermore, ammonia may re-evaporate from the inlet line walls if saturation happened previously at higher concentrations. At CLOUD, the sampling lines are attached to the chamber and cannot easily be removed during the experiments. Thus, it is not possible to quantitatively distinguish between interactions with the surface of the sampling line and the surface of the CLOUD chamber. This complicates the evaluation of the influence of the sampling line regarding the measured ammonia. One practical solution would be to report averages of the values considering the wall loss correction factor and neglecting the factor.

Sampling line losses introduce up to a factor 3 uncertainty in the ammonia measurement, corresponding to transmission efficiencies between 33.7% and 100% for walls that are a perfect sink and zero sink, respectively. Variable sampling efficiency is a general problem facing most ammonia measurements (e.g., Leifer et al. (2017)). The uncertainty is smaller for larger molecules, e.g., the sampling efficiency for triethylamine (diffusivity of 0.067 cm^2 s^{-1}, Tang et al. (2015)) is 61%. For atmospheric measurements, we suggest to use an inlet system where a short piece of the 1'' sampling line only takes the core sample flow from a large diameter inlet. A blower can generate a fast flow in the large inlet to essentially reduce the losses for the core flow to zero before it enters the actual sampling line (Berresheim et al., 2000).

3.9 Measurement of dimethylamine

The same calibration factor as derived for ammonia was used to determine the mixing ratio of dimethylamine (Section 3.5 and Table 1). This assumption can lead to uncertainties as the sensitivity of the instrument is expected to depend on the proton affinity of the measured substance (Hanson et al., 2011). To estimate the validity of this assumption, we compared the mixing ratios measured by the water cluster CI-APi-TOF with the calculated mixing ratios for a period when dimethylamine was actively injected into the CLOUD chamber. A chamber characterization for dimethylamine was already conducted by Simon et al. (2016), where the wall loss life time was determined as 432 s for conditions where the chamber walls acted as a perfect sink (12% fan speed). Additionally, as discussed in Section 3.7, we use a lifetime of 108 s at 100% fan speed (change in a factor of 4 when the fan speed is changed from 12% to 100%). The chamber dilution life time represents the maximum possible life time when wall loss would be negligible (Section 3.7). Thus, the wall loss life time used in this study gives a lower limit for dimethylamine mixing ratios in the CLOUD chamber. Figure 9a shows a period when dimethylamine was added to the chamber. Since it takes a certain time until the stainless steel pipes of the gas dilution system are saturated with dimethylamine there is a short time delay between the switching of a valve that allows dimethylamine to enter the chamber and the rise in the measured dimethylamine mixing ratio. Once the lines are conditioned and the dimethylamine is homogenously mixed into the chamber, the measured and estimated mixing ratios are generally in good agreement with each other. The response to changes of fan speed is initially sharp but gradually weakens as the walls progressively adsorb more dimethylamine. To estimate the consistency of the approach of scaling the calibration factor derived for ammonia to estimate dimethylamine mixing ratios, we use the ratio between the mixing ratio calculated for the water cluster CI-APi-TOF and the calculated mixing ratios based on

the wall loss life time for the CLOUD chamber. For these measurements, we estimated a wall loss rate in the sampling lines of ~1.96 for dimethylamine, where a diffusivity of 0.1 $cm^2\ s^{-1}$ was used (Freshour et al., 2014; Simon et al., 2016). The mean deviation between the estimated dimethylamine mixing ratio and the calculated mixing ratio is 3.48 indicating that the approach of scaling the calibration factor derived for ammonia introduces uncertainties within a factor of ~3.5. The deviations at the end of the time series shown in Figure 9a are caused by nucleation experiments in which high concentrations of other vapors are used. During these stages a significant uptake of dimethylamine on particles can explain the discrepancy between measured and expected dimethylamine. Figure 9b shows a measurement of the background dimethylamine in the chamber, measured over 5 days during CLOUD13. The mean background is ~0.14 pptv at 50 to 60% RH and temperatures of 278 to 290 K. These are similar to the backgrounds measured at 80% RH and 278 K (Table 1). The observed variations are in a range of ~0.1 to 0.3 pptv provided that the measurement is not interrupted, e.g., due to the replenishment of the water source that humidifies the flow for generating the reagent ions (which explains the first drop of the background measurement in Figure 9b). The estimated detection limits shown here are below or at similar levels compared to those reported in previous publications (You et al., 2014; Simon et al., 2016).

4. Discussion and application to ambient measurements

The present study demonstrates the successful application of a water cluster CI-APi-TOF during controlled chamber experiments to measure ammonia, dimethylamine and iodic acid. During experiments involving iodide, neutral clusters containing up to 4 iodine atoms were detected. The instrument has demonstrated unrivalled low detection limits for ammonia, as well as a fast time response and time resolution. We believe this instrument can readily be applied to atmospheric measurements. The amount of clean gas required for the corona tip (2 slm of argon and some oxygen) is rather small and can easily be supplied with gas bottles (one argon gas bottle of 50 liters at 200 bar should last about 3 days). At CLOUD there is a restriction regarding the maximum sample flow that can be drawn from the chamber. During atmospheric measurements much higher flow rates can easily be realized. Therefore, the suggested design of the inlet system using a blower and a core sample inlet should be used (Section 3.8). Furthermore, the use of an internal calibration standard would be beneficial. We have tried to add a defined mixing ratio of ND_3 to the sample flow. However, besides the expected signal at (ND_3H^+, *m*/*z* 21) further signals corresponding to NH_4^+, NDH_3+, $ND_2H_2^+$ were also present due to deuterium-hydrogen exchange, which makes this method unsuitable. Use of $^{15}NH_3$ for calibration is also unsuitable since the $^{15}NH_4^+$ signal is hard to distinguish from the comparatively high H_3O^+ signal at the same integer mass even for a high resolution mass spectrometer.

Roscioli et al. (2016) demonstrated that the addition of 1H,1H-perfluorooctylamine to the sample flow can be used to passivate an inlet, which reduces sampling line losses and sharpens the time response for ammonia measurements. Recently, Pollack et al. (2019) implemented this passivation technique for ambient measurements on an aircraft. For these measurements, a tunable infrared laser was used (TILDAS-CS, Aerodyne Inc.). We tested this passivation technique, but found it unsuitable for our instrument; the high mixing ratio of 1H,1H-perfluorooctylamine (~100 ppm to 0.1% injection into the sample flow) that is required led to excessive consumption of the reagent ions since 1H,1H-perfluorooctylamine has a high

proton affinity and is therefore also efficiently ionized by the protonated water clusters. For this reason, the passivation technique for the measurement of ammonia can in our opinion only be used with spectroscopic techniques as it was the case in the studies by Rosciolli et al. (2016) and Pollack et al. (2019).

5. Summary and Conclusion

We have described the design and performance of a novel water cluster Chemical Ionization-Atmospheric Pressure interface-Time Of Flight mass spectrometer (CI-APi-TOF) for measurements of ammonia, amines (dimethylamine) and iodine compounds. The instrument includes a new home-built cross-flow ion source operated at atmospheric pressure. The protonated water clusters ($(H_2O)_{n\geq1}H_3O^+$) selectively ionize compounds of high proton affinity at short reaction times. The instrument's response is linear up to a mixing ratio of at least 10 ppbv for ammonia when the derived calibration factor is applied to the normalized counts per second. The water cluster CI-APi-TOF was operated at the CLOUD chamber where very low background ammonia mixing ratios were measured (ca. 4 pptv at 278 K). The limit of detection (LOD) was estimated as 0.5 pptv for NH_3. To our knowledge, such a low detection limit for ammonia measurements is unprecedented. We attribute the low LOD mainly to the use of ultraclean argon (5.0 purity) as the main ion source gas for the reagent ion generation. Much higher background NH_3 was observed when nitrogen was used instead of argon. The instrument shows some sensitivity to relative humidity of the sample flow (factor 3 increase in signal from 5% to 80% RH). However, this can be readily measured and corrected. We did not explicitly demonstrate the quantitative measurement of diamines (and other amines than dimethylamine) in the present study but the instrument should also be well-suited for such measurements.

During experiments involving iodine, it was observed that the protonated water clusters can also be used to detect various iodine compounds. A total of 29 different iodine-containing compounds were identified, including iodic acid (HIO_3) and neutral clusters containing up to four iodine atoms. The water cluster CI-APi-TOF was cross-calibrated against a nitrate CI-APi-TOF measuring iodic acid. The two instruments showed exactly the same time-dependent trends. As there is no established calibration method for iodic acid, detection limits have been derived under the assumption that HIO_3 is measured with the same efficiency as sulfuric acid, for which the nitrate CI-APi-TOF was calibrated for. In this way, we estimated the LOD for iodic acid in the water cluster CI-APi-TOF to be 0.007 pptv.

Future studies will focus on the evaluation of the iodine signals and also on further signal identification in the mass spectra. Laboratory and ambient measurements indicate increased importance of ammonia for new particle formation and growth in both pristine and polluted environments. Due to the instrument characteristics, we plan to apply the method to ambient atmospheric measurements to study the influence of ammonia, amines, diamines, and iodic acid on new particle formation. The water cluster CI-APi-TOF technique is also well-suited for airborne measurements in the upper troposphere, where fast response times and low detection limits are vital (Höpfner et al., 2016).

Acknowledgements

We would like to thank CERN for the support of CLOUD with financial and technical resources. We thank the PS/SPS team from CERN for providing the CLOUD experiment with a particle beam from the proton synchroton. We also want to thank L.-P. De Menezes for providing us with a mass flow controller used during the calibrations. Next to this, we would like to thank R. Sitals, T. Keber, S. Mathot, H.E. Manninen, A. Onnela, S. K. Weber and R. Kristic for their contributions to the experiment. The discussion with Xucheng He during the creation of the paper is gratefully acknowledged. We thank C. Hüglin for providing us with the PIARRCO and its calibration unit. This work was funded by: the German Federal Ministry of Education and Research "CLOUD-16" (no. 01LK1601A), EC Horizon 2020 MSCA-ITN "CLOUD-MOTION" (no. 764991), and EC Seventh Framework Programme MC-ITN "CLOUD-TRAIN" (no. 316662).

References

Aljawhary, D., Lee, A. K. Y., and Abbatt, J. P. D.: High-resolution chemical ionization mass spectrometry (ToF-CIMS): application to study SOA composition and processing, Atmos. Meas. Tech., 6, 3211–3224, doi:10.5194/amt-6-3211-2013, 2013.

Almeida, J., Schobesberger, S., Kürten, A., Ortega, I. K., Kupiainen-Määttä, O., Praplan, A. P., Adamov, A., Amorim, A., Bianchi, F., Breitenlechner, M., David, A., Dommen, J., Donahue, N. M., Downard, A., Dunne, E., Duplissy, J., Ehrhart, S., Flagan, R. C., Franchin, A., Guida, R., Hakala, J., Hansel, A., Heinritzi, M., Henschel, H., Jokinen, T., Junninen, H., Kajos, M., Kangasluoma, J., Keskinen, H., Kupc, A., Kurtén, T., Kvashin, A. N., Laaksonen, A., Lehtipalo, K., Leiminger, M., Leppä, J., Loukonen, V., Makhmutov, V., Mathot, S., McGrath, M. J., Nieminen, T., Olenius, T., Onnela, A., Petäjä, T., Riccobono, F., Riipinen, I., Rissanen, M., Rondo, L., Ruuskanen, T., Santos, F. D., Sarnela, N., Schallhart, S., Schnitzhofer, R., Seinfeld, J. H., Simon, M., Sipilä, M., Stozhkov, Y., Stratmann, F., Tomé, A., Tröstl, J., Tsagkogeorgas, G., Vaattovaara, P., Viisanen, Y., Virtanen, A., Vrtala, A., Wagner, P. E., Weingartner, E., Wex, H., Williamson, C., Wimmer, D., Ye, P., Yli-Juuti, T., Carslaw, K. S., Kulmala, M., Curtius, J., Baltensperger, U., Worsnop, D. R., Vehkamäki, H., and Kirkby, J.: Molecular understanding of sulphuric acid-amine particle nucleation in the atmosphere, Nature, 502, 359–363, doi:10.1038/nature12663, 2013.

Baron, P. A. and Willeke, K.: Aerosol measurement: Principles, techniques, and applications, 2nd ed., Wiley, New York, xxiii, 1131, 2001.

Bell, C. L., Dhib, M., Hancock, G., Ritchie, G. A. D., van Helden, J. H., and van Leeuwen, N. J.: Cavity enhanced absorption spectroscopy measurements of pressure-induced broadening and shift coefficients in the υ 1+υ 3 combination band of ammonia, Appl. Phys. B, 94, 327–336, doi:10.1007/s00340-008-3238-5, 2009.

Benson, D. R., Markovich, A., Al-Refai, M., and Lee, S.-H.: A Chemical Ionization Mass Spectrometer for ambient measurements of Ammonia, Atmos. Meas. Tech., 3, 1075–1087, doi:10.5194/amt-3-1075-2010, 2010.

Berresheim, H., Elste, T., Plass-Dülmer, C., Eiseleb, F.L., and Tannerb, D.J.: Chemical ionization mass spectrometer for long-term measurements of atmospheric OH and H2SO4, International Journal of Mass Spectrometry, 202, 91–109, doi:10.1016/S1387-3806(00)00233-5, 2000.

Bianchi, F., Dommen, J., Mathot, S., and Baltensperger, U.: On-line determination of ammonia at low pptv mixing ratios in the CLOUD chamber, Atmos. Meas. Tech., 5, 1719–1725, doi:10.5194/amt-5-1719-2012, 2012.

Bianchi, F., Tröstl, J., Junninen, H., Frege, C., Henne, S., Hoyle, C. R., Molteni, U., Herrmann, E., Adamov, A., Bukowiecki, N., Chen, X., Duplissy, J., Gysel, M., Hutterli, M., Kangasluoma, J., Kontkanen, J., Kürten, A., Manninen, H. E., Münch, S., Peräkylä, O., Petäjä, T., Rondo, L., Williamson, C., Weingartner, E., Curtius, J., Worsnop, D. R., Kulmala, M., Dommen, J., and Baltensperger, U.: New particle formation in the free troposphere: A question of chemistry and timing, Science (New York, N.Y.), 352, 1109–1112, doi:10.1126/science.aad5456, 2016.

Bobrutzki, K. von, Braban, C. F., Famulari, D., Jones, S. K., Blackall, T., Smith, T. E. L., Blom, M., Coe, H., Gallagher, M., Ghalaieny, M., McGillen, M. R., Percival, C. J., Whitehead, J. D., Ellis, R., Murphy, J., Mohacsi, A., Pogany, A., Junninen, H., Rantanen, S., Sutton, M. A., and Nemitz, E.: Field inter-comparison of eleven atmospheric ammonia measurement techniques, Atmos. Meas. Tech., 3, 91–112, doi:10.5194/amt-3-91-2010, 2010.

Cubison, M. J. and Jimenez, J. L.: Statistical precision of the intensities retrieved from constrained fitting of overlapping peaks in high-resolution mass spectra, Atmos. Meas. Tech., 8, 2333–2345, doi:10.5194/amt-8-2333-2015, 2015.

Dias, A., Ehrhart, S., Vogel, A., Williamson, C., Almeida, J., Kirkby, J., Mathot, S., Mumford, S., and Onnela, A.: Temperature uniformity in the CERN CLOUD chamber, Atmos. Meas. Tech., 10, 5075-5088, doi: 10.5194/amt-10-5075-2017, 2017.

Dunlop, P. J. and Bignell, C. M.: Prediction of the temperature dependence of binary diffusion coefficients of gaseous systems from thermal diffusion factors and diffusion coefficients at 300 K, International Journal of Thermophysics, 18, 939–945, doi:10.1007/BF02575239, 1997.

Dunne, E. M., Gordon, H., Kürten, A., Almeida, J., Duplissy, J., Williamson, C., Ortega, I. K., Pringle, K. J., Adamov, A., Baltensperger, U., Barmet, P., Benduhn, F., Bianchi, F., Breitenlechner, M., Clarke, A., Curtius, J., Dommen, J., Donahue, N. M., Ehrhart, S., Flagan, R. C., Franchin, A., Guida, R., Hakala, J., Hansel, A., Heinritzi, M., Jokinen, T., Kangasluoma, J., Kirkby, J., Kulmala, M., Kupc, A., Lawler, M. J., Lehtipalo, K., Makhmutov, V., Mann, G., Mathot, S., Merikanto, J., Miettinen, P., Nenes, A., Onnela, A., Rap, A., Reddington, C. L. S., Riccobono, F., Richards, N. A. D., Rissanen, M. P., Rondo, L., Sarnela, N., Schobesberger, S., Sengupta, K., Simon, M., Sipilä, M., Smith, J. N., Stozkhov, Y., Tomé, A., Tröstl, J., Wagner, P. E., Wimmer, D., Winkler, P. M., Worsnop, D. R., and Carslaw, K. S.: Global atmospheric particle formation from CERN CLOUD measurements, Science (New York, N.Y.), 354, 1119–1124, doi:10.1126/science.aaf2649, 2016.

Duplissy, J., Merikanto, J., Franchin, A., Tsagkogeorgas, G., Kangasluoma, J., Wimmer, D., Vuollekoski, H.,Schobesberger, S., Lehtipalo, K., Flagan, R. C., Brus, D., Donahue, N. M., Vehkamäki, H., Almeida, J., Amorim, A., Barmet, P., Bianchi, F., Breitenlechner, M., Dunne, E. M., Guida, R., Henschel, H., Junninen, H., Kirkby, J., Kürten, A., Kupc, A., Määttänen, A., Makhmutov, V., Mathot, S., Nieminen, T., Onnela, A., Praplan, A. P., Riccobono, F., Rondo, L., Steiner, G., Tome, A., Walther, H., Baltensperger, U., Carslaw, K. S., Dommen, J., Hansel, A., Petäjä, T., Sipilä, M., Stratmann, F., Vrtala, A., Wagner, P. E., Worsnop, D. R, Curtius, J., and Kulmala, M.: Effect of ions on sulfuric acid-water binary particle formation: 2. Experimental data and comparison with QC-normalized classical nucleation theory, *J. Geophys. Res. Atmos.*, 121, 1752– 1775, doi: 10.1002/2015JD023539, 2016.

Ehn, M., Thornton, J. A., Kleist, E., Sipilä, M., Junninen, H., Pullinen, I., Springer, M., Rubach, F., Tillmann, R., Lee, B., Lopez-Hilfiker, F., Andres, S., Acir, I.-H., Rissanen, M., Jokinen, T., Schobesberger, S., Kangasluoma, J., Kontkanen, J., Nieminen, T., Kurtén, T., Nielsen, L. B., Jørgensen, S., Kjaergaard, H. G., Canagaratna, M., Maso, M. D., Berndt, T., Petäjä, T., Wahner, A., Kerminen, V.-M., Kulmala, M., Worsnop, D. R., Wildt, J., and Mentel, T. F.: A large source of low-volatility secondary organic aerosol, Nature, 506, 476 EP -, doi:10.1038/nature13032, 2014.

Eisele, F. L. and Tanner, D. J.: Measurement of the gas phase concentration of H2SO4 and methane sulfonic acid and estimates of H2SO4 production and loss in the atmosphere, Journal of Geophysical Research: Atmospheres, 98, 9001–9010, doi:10.1029/93JD00031, 1993.

Eisele, F.L. and Hanson, D.R.: First Measurement of Prenucleation Molecular Clusters, The Journal of Physical Chemistry A, 104 (4), 830-836, doi:10.1021/jp9930651, 2000.

Ellis,R. A., J. G., Pattey, E., van Haarlem, R., O'Brien, J. M., and Herndon, S. C.: Characterizing a Quantum Cascade Tunable Infrared Laser Differential Absorption Spectrometer (QC-TILDAS) for measurements of atmospheric ammonia, Atmos. Meas. Tech., 3, 397–406, https://doi.org/10.5194/amt-3-397-2010, 2010.

Elm, J., Passananti, M., Kurtén, T., and Vehkamäki, H.: Diamines Can Initiate New Particle Formation in the Atmosphere, The Journal of Physical Chemistry A, 121, 6155–6164, doi:10.1021/acs.jpca.7b05658, 2017.

Ge, X., Wexler, S.; Clegg, S.L.: Atmospheric amines- Part I. A review, Atmospheric Environment, 45, 524-546, doi: 10.1016/j.atmosenv.2010.10.012, 2011.

Good, A., Durden, D. A., and Kebarle, P.: Mechanism and Rate Constants of Ion–Molecule Reactions Leading to Formation of H + (H 2 O) n in Moist Oxygen and Air, The Journal of Chemical Physics, 52, 222–229, doi:10.1063/1.1672668, 1970.

Hansel, A., Scholz, W., Mentler, B., Fischer, L., and Berndt, T.: Detection of RO 2 radicals and other products from cyclohexene ozonolysis with NH 4 + and acetate chemical ionization mass spectrometry, Atmospheric Environment, 186, doi:10.1016/j.atmosenv.2018.04.023, 2018.

Hanson, D. R., McMurry, P. H., Jiang, J., Tanner, D., and Huey, L. G.: Ambient pressure proton transfer mass spectrometry: detection of amines and ammonia, Environmental science & technology, 45, 8881–8888, doi:10.1021/es201819a, 2011.

Haruyama, T., Namise, T., Shimoshimizu, N., Uemura, S., Takatsuji, Y., Hino, M., Yamasaki, R., Kamachi, T., and Kohno, M..: Non-catalyzed one-step synthesis of ammonia from atmospheric air and water, Green Chem., 18, 4536-4541, doi: 10.1039/C6GC01560C, 2016.

Heinritzi, M., Simon, M., Steiner, G., Wagner, A. C., Kürten, A., Hansel, A., and Curtius, J.: Characterization of the mass-dependent transmission efficiency of a CIMS, Atmos. Meas. Tech., 9, 1449–1460, doi:10.5194/amt-9-1449-2016, 2016.

Höpfner, M., Volkamer, R., Grabowski, U., Grutter, M., Orphal, J., Stiller, G., Clarmann, T. von, and Wetzel, G.: First detection of ammonia (NH3) in the Asian summer monsoon upper troposphere, Atmos. Chem. Phys., 16, 14357–14369, doi:10.5194/acp-16-14357-2016, 2016.

Jen, C. N., Bachman, R., Zhao, J., McMurry, P. H., and Hanson, D. R.: Diamine-sulfuric acid reactions are a potent source of new particle formation, Geophys. Res. Lett., 43, 867–873, doi:10.1002/2015GL066958, 2016.

Jimenez, J. L., Canagaratna, M. R., Donahue, N. M., Prevot, A. S. H., Zhang, Q., Kroll, J. H., DeCarlo, P. F., Allan, J. D., Coe, H., Ng, N. L., Aiken, A. C., Docherty, K. S., Ulbrich, I. M., Grieshop, A. P., Robinson, A. L., Duplissy, J., Smith, J. D., Wilson, K. R., Lanz, V. A., Hueglin, C., Sun, Y. L., Tian, J., Laaksonen, A., Raatikainen, T., Rautiainen, J., Vaattovaara, P., Ehn, M., Kulmala, M., Tomlinson, J. M., Collins, D. R., Cubison, M. J., Dunlea, J., Huffman, J. A.,

Onasch, T. B., Alfarra, M. R., Williams, P. I., Bower, K., Kondo, Y., Schneider, J., Drewnick, F., Borrmann, S., Weimer, S., Demerjian, K., Salcedo, D., Cottrell, L., Griffin, R., Takami, A., Miyoshi, T., Hatakeyama, S., Shimono, A., Sun, J. Y., Zhang, Y. M., Dzepina, K., Kimmel, J. R., Sueper, D., Jayne, J. T., Herndon, S. C., Trimborn, A. M., Williams, L. R., Wood, E. C., Middlebrook, A. M., Kolb, C. E., Baltensperger, U., and Worsnop, D. R.: Evolution of Organic Aerosols in the Atmosphere, Science (New York, N.Y.), 326, 1525–1529, doi:10.1126/science.1180353, 2009.

Jokinen, T., Sipilä, M., Junninen, H., Ehn, M., Lönn, G., Hakala, J., Petäjä, T., Mauldin III, R. L., Kulmala, M., and Worsnop, D. R.: Atmospheric sulphuric acid and neutral cluster measurements using CI-APi-TOF, Atmos. Chem. Phys., 12, 4117–4125, doi:10.5194/acp-12-4117-2012, 2012.

Jokinen, T., Sipilä, M., Kontkanen, J., Vakkari, V., Tisler, P., Duplissy, E.-M., Junninen, H., Kangasluoma, J., Manninen, H. E., Petäjä, T., Kulmala, M., Worsnop, D. R., Kirkby, J., Virkkula, A., and Kerminen, V.-M.: Ion-induced sulfuric acid\textendashammonia nucleation drives particle formation in coastal Antarctica, Science Advances, 4, doi:10.1126/sciadv.aat9744, 2018.

Kebarle, P.: Higher-Order Reactions--Ion Clusters and Ion Solvation, in: Ion-Molecule Reactions: Volume 1, Franklin, J. L. (Ed.), Springer US, Boston, MA, 315–362, 1972.

Kirkby, J., Curtius, J., Almeida, J., Dunne, E., Duplissy, J., Ehrhart, S., Franchin, A., Gagné, S., Ickes, L., Kürten, A., Kupc, A., Metzger, A., Riccobono, F., Rondo, L., Schobesberger, S., Tsagkogeorgas, G., Wimmer, D., Amorim, A., Bianchi, F., Breitenlechner, M., David, A., Dommen, J., Downard, A., Ehn, M., Flagan, R. C., Haider, S., Hansel, A., Hauser, D., Jud, W., Junninen, H., Kreissl, F., Kvashin, A., Laaksonen, A., Lehtipalo, K., Lima, J., Lovejoy, E. R., Makhmutov, V., Mathot, S., Mikkilä, J., Minginette, P., Mogo, S., Nieminen, T., Onnela, A., Pereira, P., Petäjä, T., Schnitzhofer, R., Seinfeld, J. H., Sipilä, M., Stozhkov, Y., Stratmann, F., Tomé, A., Vanhanen, J., Viisanen, Y., Vrtala, A., Wagner, P. E., Walther, H., Weingartner, E., Wex, H., Winkler, P. M., Carslaw, K. S., Worsnop, D. R., Baltensperger, U., and Kulmala, M.: Role of sulphuric acid, ammonia and galactic cosmic rays in atmospheric aerosol nucleation, Nature, 476, 429 EP -, doi:10.1038/nature10343, 2011.

Kirkby, J., Duplissy, J., Sengupta, K., Frege, C., Gordon, H., Williamson, C., Heinritzi, M., Simon, M., Yan, C., Almeida, J., Tröstl, J., Nieminen, T., Ortega, I. K., Wagner, R., Adamov, A., Amorim, A., Bernhammer, A.-K., Bianchi, F., Breitenlechner, M., Brilke, S., Chen, X., Craven, J., Dias, A., Ehrhart, S., Flagan, R. C., Franchin, A., Fuchs, C., Guida, R., Hakala, J., Hoyle, C. R., Jokinen, T., Junninen, H., Kangasluoma, J., Kim, J., Krapf, M., Kürten, A., Laaksonen, A., Lehtipalo, K., Makhmutov, V., Mathot, S., Molteni, U., Onnela, A., Peräkylä, O., Piel, F., Petäjä, T., Praplan, A. P., Pringle, K., Rap, A., Richards, N. A. D., Riipinen, I., Rissanen, M. P., Rondo, L., Sarnela, N., Schobesberger, S., Scott, C. E., Seinfeld, J. H., Sipilä, M., Steiner, G., Stozhkov, Y., Stratmann, F., Tomé, A., Virtanen, A., Vogel, A. L., Wagner, A. C., Wagner, P. E., Weingartner, E., Wimmer, D., Winkler, P. M., Ye, P., Zhang, X., Hansel, A., Dommen, J., Donahue, N. M., Worsnop, D. R., Baltensperger, U., Kulmala, M., Carslaw, K. S., and Curtius, J.: Ion-induced nucleation of pure biogenic particles, Nature, 533, 521 EP -, doi:10.1038/nature17953, 2016.

Kupc, A., Amorim, A., Curtius, J., Danielczok, A., Duplissy, J., Ehrhart, S., Walther, H., Ickes, L., Kirkby, J., Kürten, A., Lima, J. M., Mathot, S., Minginette, P., Onnela, A., Rondo, and Rondo, L.: A fibre-optic UV system for H2SO4 production in aerosol chambers causing minimal thermal effects, Journal of Aerosol Science, 42, 532–543, doi:10.1016/j.jaerosci.2011.05.001, 2011.

Kurtén, T., Loukonen, V., Vehkamäki, H., and Kulmala, M.: Amines are likely to enhance neutral and ion-induced sulfuric acid-water nucleation in the atmosphere more effectively than ammonia, Atmos. Chem. Phys. Discuss., 8, 7455–7476, doi:10.5194/acpd-8-7455-2008, 2008.

Kürten, A.: New particle formation from sulfuric acid and ammonia: nucleation and growth model based on thermodynamics derived from CLOUD measurements for a wide range of conditions, Atmos. Chem. Phys.,19, 5033-5050, doi:10.5194/acp-19-5033-2019, 2019.

Kürten, A., Bergen, A., Heinritzi, M., Leiminger, M., Lorenz, V., Piel, F., Simon, M., Sitals, R., Wagner, A. C., and Curtius, J.: Observation of new particle formation and measurement of sulfuric acid, ammonia, amines and highly oxidized organic molecules at a rural site in central Germany, Atmos. Chem. Phys., 16, 12793–12813, doi:10.5194/acp-16-12793-2016, 2016b.

Kürten, A., Bianchi, F., Almeida, J., Kupiainen-Määttä, O., Dunne, E. M., Duplissy, J., Williamson, C., Barmet, P., Breitenlechner, M., Dommen, J., Donahue, N. M., Flagan, R. C., Franchin, A., Gordon, H., Hakala, J., Hansel, A., Heinritzi, M., Ickes, L., Jokinen, T., Kangasluoma, J., Kim, J., Kirkby, J., Kupc, A., Lehtipalo, K., Leiminger, M., Makhmutov, V., Onnela, A., Ortega, I. K., Petäjä, T., Praplan, A. P., Riccobono, F., Rissanen, M. P., Rondo, L., Schnitzhofer, R., Schobesberger, S., Smith, J. N., Steiner, G., Stozhkov, Y., Tomé, A., Tröstl, J., Tsagkogeorgas, G., Wagner, P. E., Wimmer, D., Ye, P., Baltensperger, U., Carslaw, K., Kulmala, M., and Curtius, J.: Experimental particle formation rates spanning tropospheric sulfuric acid and ammonia abundances, ion production rates, and temperatures, J. Geophys. Res. Atmos., 121, 12,377-12,400, doi:10.1002/2015JD023908, 2016a.

Kürten, A., Jokinen, T., Simon, M., Sipilä, M., Sarnela, N., Junninen, H., Adamov, A., Almeida, J., Amorim, A., Bianchi, F., Breitenlechner, M., Dommen, J., Donahue, N. M., Duplissy, J., Ehrhart, S., Flagan, R. C., Franchin, A., Hakala, J., Hansel, A., Heinritzi, M., Hutterli, M., Kangasluoma, J., Kirkby, J., Laaksonen, A., Lehtipalo, K., Leiminger, M., Makhmutov, V., Mathot, S., Onnela, A., Petäjä, T., Praplan, A. P., Riccobono, F., Rissanen, M. P., Rondo, L., Schobesberger, S., Seinfeld, J. H., Steiner, G., Tomé, A., Tröstl, J., Winkler, P. M., Williamson, C., Wimmer, D., Ye, P., Baltensperger, U., Carslaw, K. S., Kulmala, M., Worsnop, D. R., and Curtius, J.: Neutral molecular cluster formation of sulfuric acid-dimethylamine observed in real time under atmospheric conditions, Proceedings of the National Academy of Sciences of the United States of America, 111, 15019–15024, doi:10.1073/pnas.1404853111, 2014.

Kürten, A., Rondo, L., Ehrhart, S., and Curtius, J.: Performance of a corona ion source for measurement of sulfuric acid by chemical ionization mass spectrometry, Atmos. Meas. Tech., 4, 437–443, doi:10.5194/amt-4-437-2011, 2011.

Kürten, A., Rondo, L., Ehrhart, S., and Curtius, J.: Calibration of a Chemical Ionization Mass Spectrometer for the Measurement of Gaseous Sulfuric Acid, The Journal of Physical Chemistry A, 116, 6375–6386, doi:10.1021/jp212123n, 2012.

Lehtipalo, K., Yan, C., Dada, L., Bianchi, F., Xiao, M., Wagner, R., Stolzenburg, D., Ahonen, L. R., Amorim, A., Baccarini, A., Bauer, P. S., Baumgartner, B., Bergen, A., Bernhammer, A.-K., Breitenlechner, M., Brilke, S., Buchholz, A., Mazon, S. B., Chen, D., Chen, X., Dias, A., Dommen, J., Draper, D. C., Duplissy, J., Ehn, M., Finkenzeller, H., Fischer, L., Frege, C., Fuchs, C., Garmash, O., Gordon, H., Hakala, J., He, X., Heikkinen, L., Heinritzi, M., Helm, J. C., Hofbauer, V., Hoyle, C. R., Jokinen, T., Kangasluoma, J., Kerminen, V.-M., Kim, C., Kirkby, J., Kontkanen, J., Kürten, A., Lawler, M. J., Mai, H., Mathot, S., Mauldin, R. L., Molteni, U., Nichman, L., Nie, W., Nieminen, T., Ojdanic, A., Onnela, A., Passananti, M., Petäjä, T., Piel, F., Pospisilova, V., Quéléver, L. L. J., Rissanen, M. P., Rose, C., Sarnela, N., Schallhart, S., Schuchmann, S., Sengupta, K., Simon, M., Sipilä, M., Tauber, C., Tomé, A., Tröstl, J., Väisänen, O., Vogel, A. L., Volkamer, R., Wagner, A. C., Wang, M., Weitz, L., Wimmer, D., Ye, P., Ylisirniö, A., Zha, Q., Carslaw, K. S., Curtius, J., Donahue, N. M., Flagan, R. C., Hansel, A., Riipinen, I., Virtanen, A., Winkler, P. M., Baltensperger, U., Kulmala, M., and Worsnop, D. R.: Multicomponent new particle formation from sulfuric acid, ammonia, and biogenic vapors, Science Advances, 4, doi:10.1126/sciadv.aau5363, 2018.

Leifer, I., Melton, C., Tratt, D. M., Buckland, K. N., Clarisse, L., Coheur, P., Frash, J., Gupta, M., Johnson, P. D., Leen, J. B., van Damme, M., Whitburn, S., and Yurganov, L.: Remote sensing and in situ measurements of methane and ammonia emissions from a megacity dairy complex: Chino, CA, Environmental pollution (Barking, Essex 1987), 221, 37–51, doi:10.1016/j.envpol.2016.09.083, 2017.

Martin, N. A., Ferracci, V., Cassidy, N., and Hoffnagle, J. A.: The application of a cavity ring-down spectrometer to measurements of ambient ammonia using traceable primary standard gas mixtures, Appl. Phys. B, 122, 219, doi:10.1007/s00340-016-6486-9, 2016.

Murphy, D. M. and Koop, T.: Review of the vapour pressures of ice and supercooled water for atmospheric applications, Quarterly Journal of the Royal Meteorological Society, 131, 1539–1565, doi:10.1256/qj.04.94, 2005.

Norman, M., Hansel, A., and Wisthaler, A.: O2+ as reagent ion in the PTR-MS instrument: Detection of gas-phase ammonia, International Journal of Mass Spectrometry, 265, 382–387, doi:10.1016/j.ijms.2007.06.010, 2007.

Norman, M., Spierig, C., Wolff, V., Trebs, I., Flechard, C., Wisthaler, A., Schnitzhofer, R., Hansel, A., and Neftel, A.: Intercomparison of ammonia measurement techniques at an intensively managed grassland site (Oensingen, Switzerland), Atmospheric Chemistry and Physics Discussions, v.8, 19791-19818 (2008), 2009.

Nowak, J. B., Huey, L. G., Eisele, F. L., Tanner, D. J., Mauldin, R. L., Cantrell, C., Kosciuch, E., and Davis, D., Chemical ionization mass spectrometry technique for the detection of dimethylsulfoxide and ammonia, J. Geophys. Res., 107(D18), 4363, doi:10.1029/2001JD001058, 2002.

Nowak, J. B., Huey, L. G., Russel, A.G., Tian D., Neuman, J.A., Orsini, D., Sjostedt, S.J., Sullivan, A.P., Tanner, D.J., Weber, R.J., Nenes, A.,Edgerton, E., and Fehsenfeld, F.C., Analysis of urban gas phase ammonia measurements from

the 2002 Atlanta Aerosol Nucleation and Real-Time Characterization Experiment (ANARChE), J. Geophys. Res., 111, D17308, doi:10.1029/2006JD007113, 2006.

Nowak, J., Neuman, J., Bahreini, R., A. Brock, C., M. Middlebrook, A., G. Wollny, A., Holloway, J., Peischl, J., B. Ryerson, T., and Fehsenfeld, F.: Airborne observations of ammonia and ammonium nitrate formation over Houston, Texas, J. Geophys. Res., 115, doi:10.1029/2010JD014195, 2010.

Nowak, J., Neuman, J., Kozai, K., G. Huey, L., Tanner, D., Holloway, J., B. Ryerson, T., Frost, G., McKeen, S., and Fehsenfeld, F.: A chemical ionization mass spectrometry technique for airborne measurements of ammonia, J. Geophys. Res., 112, D10S02, doi:10.1029/2006JD007589, 2007.

Pollack, I. B., Lindaas, J., Roscioli, J. R., Agnese, M., Permar, W., Hu, L., and Fischer, E. V.: Evaluation of ambient ammonia measurements from a research aircraft using a closed-path QC-TILDAS spectrometer operated with active continuous passivation, Atmos. Meas. Tech. Discuss., https://doi.org/10.5194/amt-2019-11, in review, 2019.

Pozzer, A., Tsimpidi, A. P., Karydis, V. A., Meij, A. de, and Lelieveld, J.: Impact of agricultural emission reductions on fine-particulate matter and public health, Atmos. Chem. Phys., 17, 12813–12826, doi:10.5194/acp-17-12813-2017, 2017.

Roscioli, J. R., Zahniser, M. S., Nelson, D. D., Herndon, S. C., and Kolb, C. E.: New Approaches to Measuring Sticky Molecules: Improvement of Instrumental Response Times Using Active Passivation, The journal of physical chemistry. A, 120, 1347–1357, doi:10.1021/acs.jpca.5b04395, 2016.

Simon, M., Heinritzi, M., Herzog, S., Leiminger, M., Bianchi, F., Praplan, A., Dommen, J., Curtius, J., and Kürten, A.: Detection of dimethylamine in the low pptv range using nitrate chemical ionization atmospheric pressure interface time-of-flight (CI-APi-TOF) mass spectrometry, Atmos. Meas. Tech., 9, 2135–2145, doi:10.5194/amt-9-2135-2016, 2016.

Sipilä, M., Sarnela, N., Jokinen, T., Henschel, H., Junninen, H., Kontkanen, J., Richters, S., Kangasluoma, J., Franchin, A., Peräkylä, O., Rissanen, M. P., Ehn, M., Vehkamäki, H., Kurten, T., Berndt, T., Petäjä, T., Worsnop, D., Ceburnis, D., Kerminen, V.-M., Kulmala, M., and O'Dowd, C.: Molecular-scale evidence of aerosol particle formation via sequential addition of HIO3, Nature, 537, 532 EP -, doi:10.1038/nature19314, 2016.

Sipilä, M., Sarnela, N., Jokinen, T., Junninen, H., Hakala, J., Rissanen, M. P., Praplan, A., Simon, M., Kürten, A., Bianchi, F., Dommen, J., Curtius, J., Petäjä, T., and Worsnop, D. R.: Bisulfate – cluster based atmospheric pressure chemical ionization mass spectrometer for high-sensitivity (< 100 ppqV) detection of atmospheric dimethyl amine: proof-of-concept and first ambient data from boreal forest, Atmos. Meas. Tech., 8, 4001–4011, doi:10.5194/amt-8-4001-2015, 2015.

Skrotzki, J.: High-accuracy multiphase humidity measurements using TDLAS: application to the investigation of ice growth in simulated cirrus clouds, Ruperto-Carola University of Heidelberg, Heidelberg, 2012.

Stark, H., Yatavelli, R. L.N., Thompson, S. L., Kimmel, J. R., Cubison, M. J., Chhabra, P. S., Canagaratna, M. R., Jayne, J. T., Worsnop, D.R. and Jimenez, J. L.: Methods to extract molecular and bulk chemical information from series of

complex mass spectra with limited mass resolution, International Journal of Mass Spectrometry, 389, 26–38, doi:10.1016/j.ijms.2015.08.011, 2015.

Sunner, J., Nicol, G., and Kebarle, P.: Factors determining relative sensitivity of analytes in positive mode atmospheric pressure ionization mass spectrometry, Analytical Chemistry, 60, 1300–1307, doi:10.1021/ac00164a012, 1988.

Tang, M. J., Shiraiwa, M., Pöschl, U., Cox, R. A., and Kalberer, M.: Compilation and evaluation of gas phase diffusion coefficients of reactive trace gases in the atmosphere: Volume 2. Diffusivities of organic compounds, pressure-normalised mean free paths, and average Knudsen numbers for gas uptake calculations, Atmos. Chem. Phys., 15, 5585-5598, https://doi.org/10.5194/acp-15-5585-2015, 2015.

Timonen, H., Cubison, M., Aurela, M., Brus, D., Lihavainen, H., Hillamo, R., Canagaratna, M., Nekat, B., Weller, R., Worsnop, D., and Saarikoski, S.: Applications and limitations of constrained high-resolution peak fitting on low resolving power mass spectra from the ToF-ACSM, Atmos. Meas. Tech., 9, 3263–3281, doi:10.5194/amt-9-3263-2016, 2016.

Vaittinen, O., Metsälä, M., Persijn, S., Vainio, M., and Halonen, L.: Adsorption of ammonia on treated stainless steel and polymer surfaces, Appl. Phys. B, 115, doi:10.1007/s00340-013-5590-3, 2014.

Verriele, M., Plaisance, H., Depelchin, L., Benchabane, S., Locoge, N., and Meunier, G.: Determination of 14 amines in air samples using midget impingers sampling followed by analysis with ion chromatography in tandem with mass spectrometry, Journal of environmental monitoring JEM, 14, 402–408, doi:10.1039/c2em10636a, 2012.

Viggiano, A. A., Seeley, J. V., Mundis, P. L., Williamson, J. S., and Morris, R. A.: Rate constants for the reactions of $XO_3^-(H_2O)_n$ (X = C, HC, and N) and $NO_3^-(H_3O)_n$ with H_2SO_4: implications for atmospheric detection of H_2SO_4, J. Chem. Phys. A, 101, 8275-8278, doi: 10.1021/jp971768h, 1997.

W.J. Massman: A review of the molecular diffusivities of H2O, CO2, CH4, CO, O3, SO2, NH3, N2O, NO, and NO2 in air, O2 and N2 near STP, Atmospheric Environment, 32, 1111–1127, doi:10.1016/S1352-2310(97)00391-9, 1998.

Wang, S., Nan, J., Shi, C., Fu, Q., Gao, S., Wang, D., Cui, H., Saiz-Lopez, A., and Zhou, B.: Atmospheric ammonia and its impacts on regional air quality over the megacity of Shanghai, China, Scientific reports, 5, 15842, doi:10.1038/srep15842, 2015.

Weissler, G. L.: Positive and Negative Point-to-Plane Corona in Pure and Impure Hydrogen, Nitrogen, and Argon, Phys. Rev., 63, 96–107, doi:10.1103/PhysRev.63.96, 1943.

Wilkinson, G. N. and Rogers, C. E.: Symbolic Description of Factorial Models for Analysis of Variance, Journal of the Royal Statistical Society. Series C (Applied Statistics), 22, 392–399, doi:10.2307/2346786, 1973.

Yan, C., Dada, L., Rose, C., Jokinen, T., Nie, W., Schobesberger, S., Junninen, H., Lehtipalo, K., Sarnela, N., Makkonen, U., Garmash, O., Wang, Y., Zha, Q., Paasonen, P., Bianchi, F., Sipilä, M., Ehn, M., Petäjä, T., Kerminen, V.-M., Worsnop, D. R., and Kulmala, M.: The role of H2SO4-NH3 anion clusters in ion-induced aerosol nucleation mechanisms in the boreal forest, Atmos. Chem. Phys., 18, 13231–13243, doi:10.5194/acp-18-13231-2018, 2018.

Yao, L., Wang, M.-Y., Wang, X.-K., Liu, Y.-J., Chen, H.-F., Zheng, J., Nie, W., Ding, A.-J., Geng, F.-H., Wang, D.-F., Chen, J.-M., Worsnop, D. R., and Wang, L.: Detection of atmospheric gaseous amines and amides by a high-resolution time-of-flight chemical ionization mass spectrometer with protonated ethanol reagent ions, Atmos. Chem. Phys., 16, 14527–14543, doi:10.5194/acp-16-14527-2016, 2016.

Yokelson, R. J.: Evaluation of adsorption effects on measurements of ammonia, acetic acid, and methanol, J. Geophys. Res., 108, 75, doi:10.1029/2003JD003549, 2003.

You, Y., Kanawade, V. P., Gouw, J. A. de, Guenther, A. B., Madronich, S., Sierra-Hernández, M. R., Lawler, M., Smith, J. N., Takahama, S., Ruggeri, G., Koss, A., Olson, K., Baumann, K., Weber, R. J., Nenes, A., Guo, H., Edgerton, E. S., Porcelli, L., Brune, W. H., Goldstein, A. H., and Lee, S.-H.: Atmospheric amines and ammonia measured with a chemical ionization mass spectrometer (CIMS), Atmos. Chem. Phys., 14, 12181–12194, doi:10.5194/acp-14-12181-2014, 2014.

Yu, F., Nadykto, A. B., Herb, J., Luo, G., Nazarenko, K. M., and Uvarova, L. A.: H2SO4–H2O–NH3 ternary ion-mediated nucleation (TIMN): kinetic-based model and comparison with CLOUD measurements, Atmos. Chem. Phys., 18, 17451–17474, doi:10.5194/acp-18-17451-2018, 2018.

Zhao, J. and Zhang, R.: Proton transfer reaction rate constants between hydronium ion (H3O+) and volatile organic compounds, Atmospheric Environment, 38, 2177–2185, doi:10.1016/j.atmosenv.2004.01.019, 2004.

Table 1. Estimated limits of detection (LOD) for some compounds with high proton affinity, and for iodic acid, measured with the water cluster CI-APi-TOF. The LOD is derived by background measurements at the CLOUD chamber, where LOD = 3•σ (You et al., 2014). σ is defined as the standard deviation of the background signal. The detection limits are based on a measurement at 278 K and 80% RH (1 minute averaging time). The measured instrumental background mixing ratios (mean values) during this time period are also indicated.

Detected compound	**LOD (pptv)**	**Instrumental background (pptv)**	**Measured *m/z* values (Th)**
NH_3 (ammonia)	0.5 ± 0.05	3.73 ± 0.35	18.0338 (NH_4^+); 36.0444 ($(H_2O)NH_4^+$)
$(CH_3)_2NH$ (dimethylamine)*	0.047*	0.058*	46.0651 ($(CH_3)_2NH_2^+$)
HIO_3 (iodic acid)**	0.007**	< LOD**	176.9043 ($(HIO_3)H^+$); 194.9149 ($(HIO_3)H_3O^+$)

*Amine mixing ratios are estimated using the same calibration factor derived for ammonia. This can cause uncertainties. The applicability of this assumption is discussed in Section 3.9.

**Iodic acid mixing ratios are derived from an inter-comparison with a nitrate CI-APi-TOF, which evaluates HIO_3 based on a calibration factor derived for sulfuric acid. This assumption can lead to uncertainties but is necessary because no direct calibration method exists for such low gas phase HIO_3 concentrations.

Table 2. Iodine-containing compounds (atomic composition), together with their *m*/*z* values, identified in the water cluster CI-APi-TOF spectra during the CLOUD13 campaign.

Detected compound	***m*/*z* value (Th)**
I^+	126.9039
IO^+	142.8988
HIO^+	143.9067
IO_2^+	158.8938
$H_2IO_2^+$	160.9094
$H_3IO_2^+$	161.9172
$H_4IO_2^+$	162.9251
HIO_3^+	175.8965
$H_2IO_3^+$	176.9043
$H_3IO_3^+$	177.9121
$H_4IO_3^+$	178.9200
$H_4IO_4^+$	194.9149
$H_6IO_5^+$	212.9254
I_2^+	253.8084
$HI_2O_5^+$	334.7908
$H_3I_2O_5^+$	336.8064
$H_3I_2O_6^+$	352.8014
$H_5I_2O_6^+$	354.8170
$H_5I_2O_7^+$	370.8119
$H_2I_3O_7^+$	494.6929
$HI_3O_8^+$	509.6800
$H_2I_3O_8^+$	510.6878
$H_4I_3O_8^+$	512.7035
$H_4I_3O_9^+$	528.6984
$HI_4O_8^+$	636.5845
$HI_4O_9^+$	652.5794
$H_3I_4O_9^+$	654.5950
$H_3I_4O_{10}^+$	670.5900
$H_3I_4O_{11}^+$	686.5849

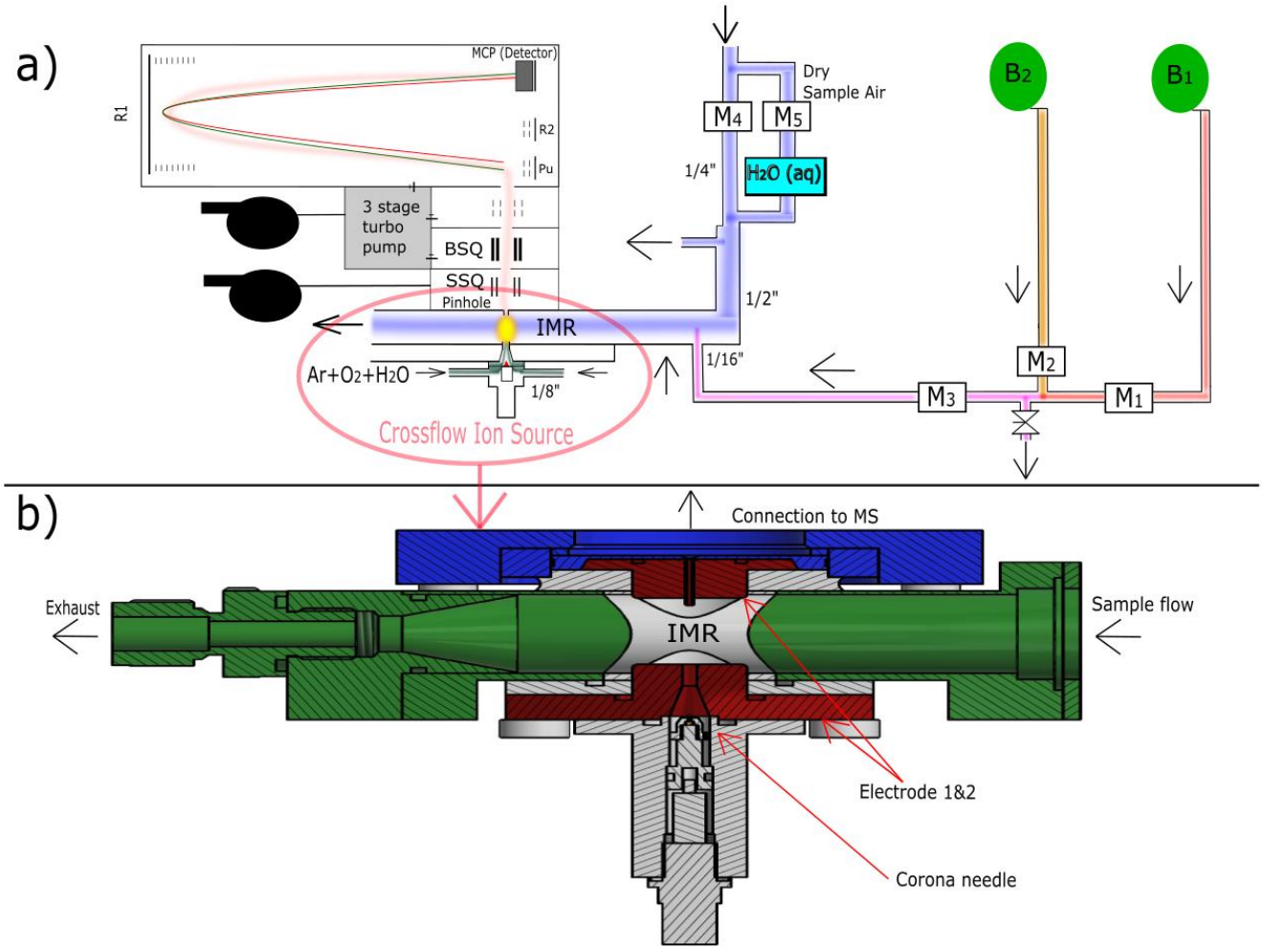

870 **Figure 1:** The experimental setup of the water cluster CI-APi-TOF during ammonia calibration is shown in panel a). The blue color indicates the sample flow. It consists of a mixture of 80% nitrogen and 20% oxygen. A portion of the sample flow can be humidified with a water bubbler (H_2O aq) to achieve different relative humidities. B_1 represents the ammonia gas bottle, while B_2 represents a gas bottle containing pure nitrogen. There are five mass flow controllers (MFCs; labeled as $M_{1\text{-}5}$) allowing two dilution steps. Three MFCs (M_1, M_2, M_3) control the amount of ammonia that is added through a 1/16'' capillary into the center of the sample flow, where the second dilution stage occurs. 875 The reagent ions (i.e., protonated water clusters) are produced when the ion source gas (argon, oxygen, water vapor) passes a corona needle at a positive high voltage (detailed in panel b). The calibration setup is disconnected during the measurements at the CLOUD chamber to reduce backgrounds (leakage from the 1/16'' capillary). Details of the ion source used during CLOUD13 are shown in panel b). The primary ions are guided towards the sample flow using a counter electrode (Electrode 1). Additionally, a funnel is used to accelerate the primary ions towards the sample flow. A second electrode (Electrode 2) is installed directly in front of the pinhole of the mass spectrometer. The ions 880 enter the mass spectrometer through a capillary on the top of Electrode 2.

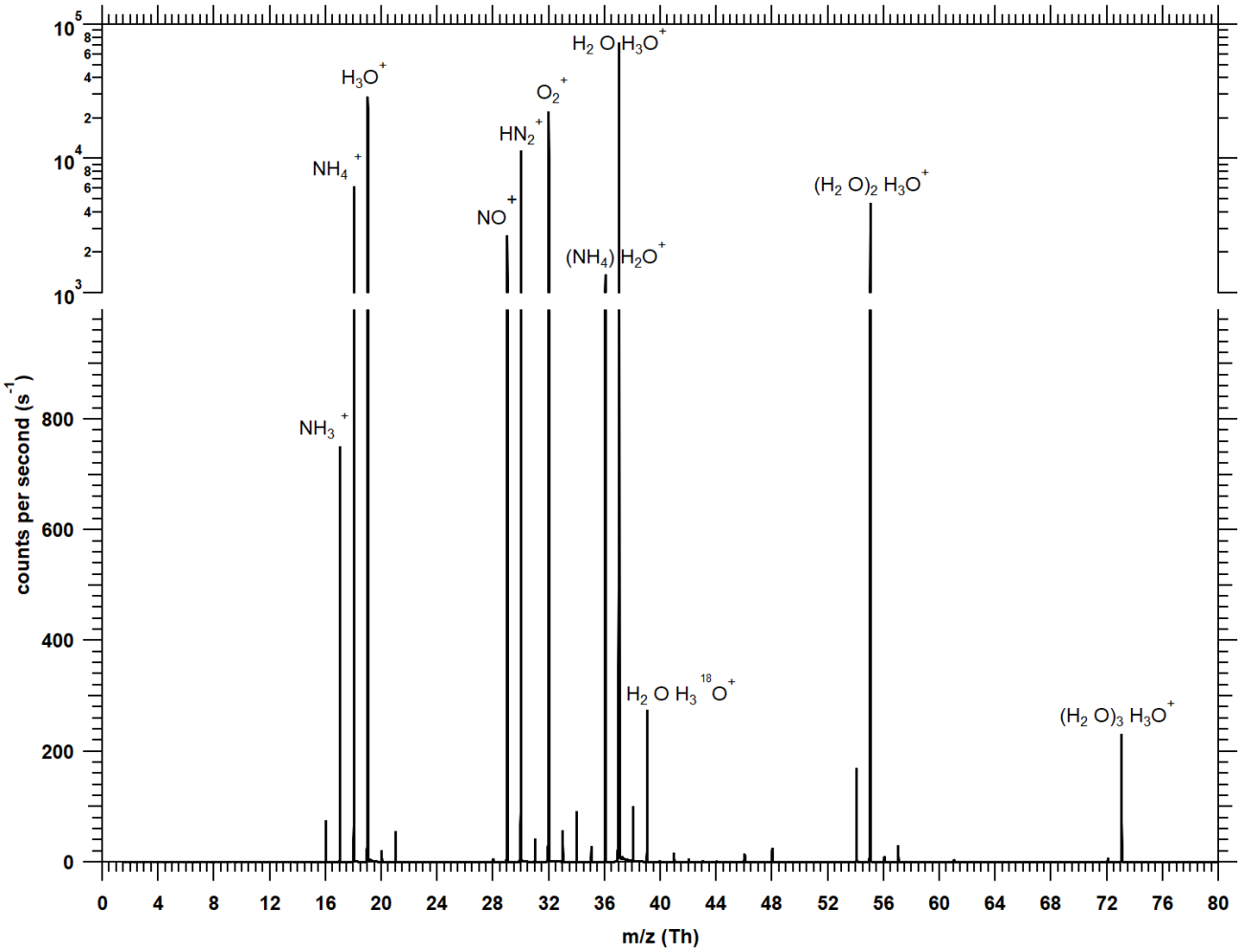

885

Figure 2: Typical mass spectrum recorded with the water cluster CI-APi-TOF when about 10 ppbv of ammonia are added during a calibration. Signals below 1000 counts per second are shown on a linear scale, while the dominant signals (> 1000 cps) are shown on a logarithmic scale. To calculate the ammonia mixing ratio, the product ion signals (NH_4^+ and $(H_2O)NH_4^+$) are normalized against the most prominent reagent ion signals (H_3O^+, $(H_2O)H_3O^+$, $(H_2O)_2H_3O^+$, $(H_2O)_3H_3O^+$). Larger water clusters are probably also present in the ion-
890 molecule reaction zone but a significant fraction of water evaporates upon crossing the pinhole at the atmospheric pressure interface of the instrument. Background peaks from N_2H^+, NO^+ and O_2^+ are always present but are neglected in the data evaluation. Due to the short reaction time (< 1 ms) in the ion-molecule reaction zone, the count rates of the reagent ions dominate the spectrum even at high ammonia mixing ratios near 10 ppbv.

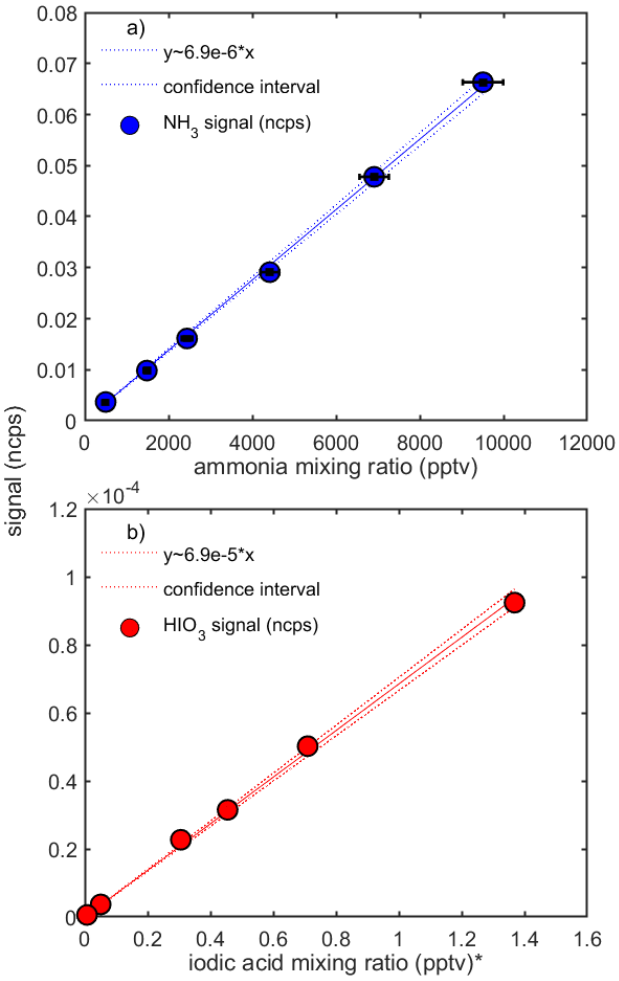

Figure 3: Calibration curves for ammonia (a) and iodic acid (b) at 40% relative humidity. The *y*-axes show the normalized counts per second (ncps) measured with the water cluster CI-APi-TOF. The ammonia mixing ratios are determined from the calibration set-up and the iodic acid mixing ratios are taken from simultaneous measurements with a nitrate CI-APi-TOF at the CLOUD chamber. The systematic uncertainty of the iodic acid mixing ratios is estimated as +100%/-50% (Sipilä et al., 2016). The inverse slopes from the linear fits yield the calibration factors (see equation (1) and (2)).

*Note that the iodic acid mixing ratio is derived by applying a calibration factor for sulfuric acid to the nitrate CI-APi-TOF data.

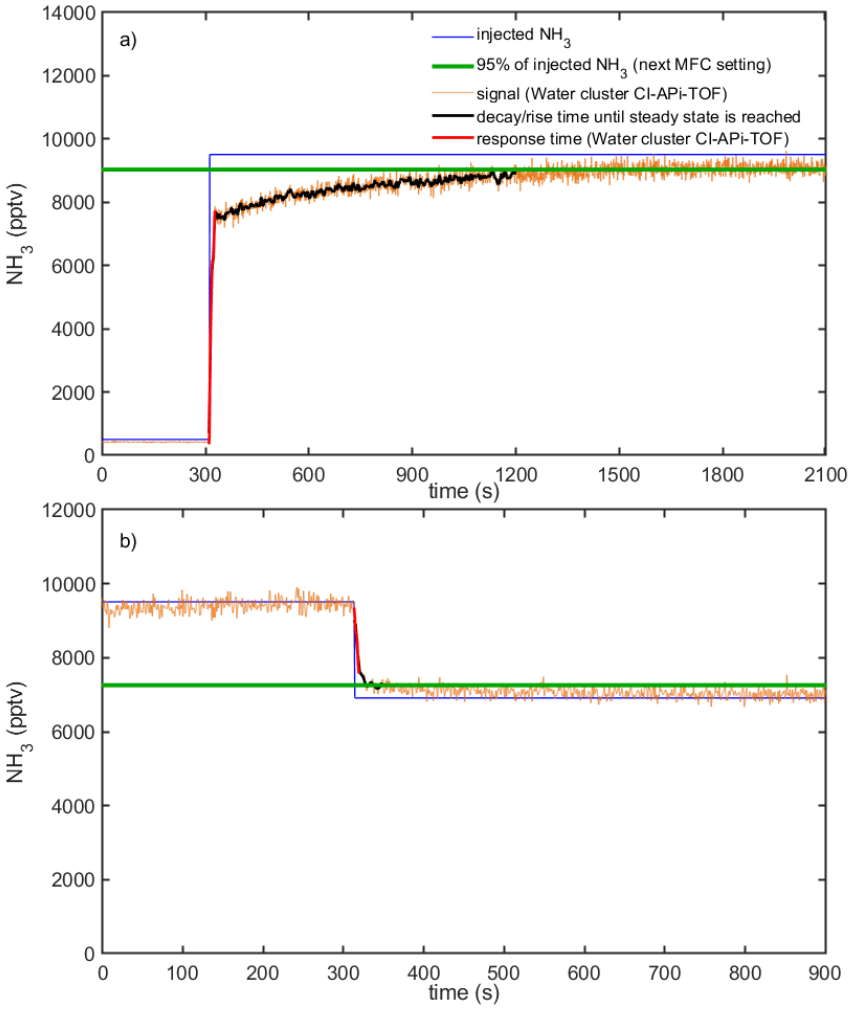

Figure 4: Response time of the water cluster CI-APi-TOF during calibrations at 60% RH. The injected ammonia mixing ratio from MFC settings is shown by the blue line. The signal of the water cluster CI-APi-TOF is shown by the orange line (here the data are shown with a 1 s time resolution, i. e., no time-averaging is applied). The green line represents 95% of the mixing ratio being applied with the next MFC setting. The black line shows the response time until a steady state (panel a) or 95% of the final measured concentration is reached (panel b). The response time is the sum of the response time of the water cluster CI-APi-TOF (red line) and the (slower) response time for the lines to reach a steady state where the walls are conditioned.

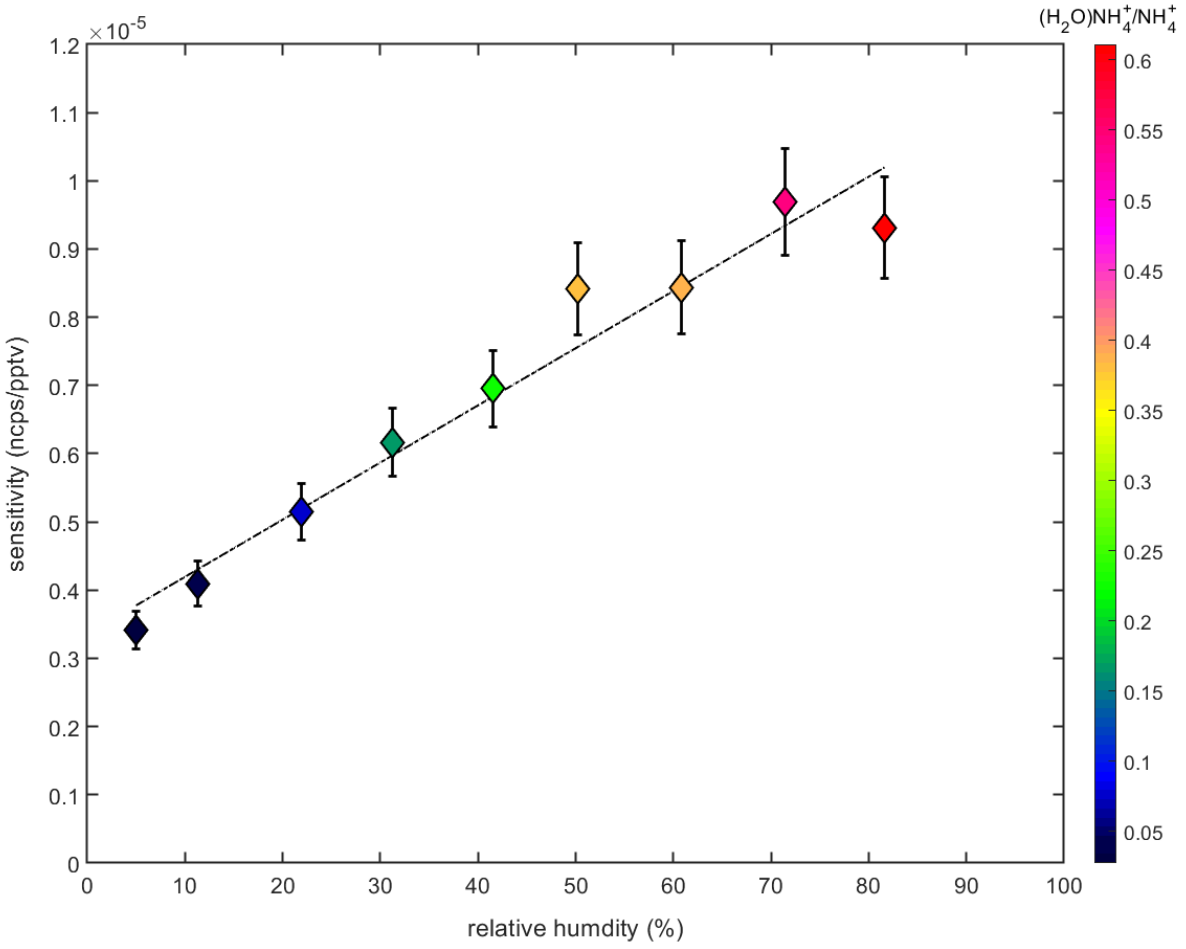

Figure 5: Dependency of the ammonia sensitivity as a function of the relative humidity (in %). A linear increase with relative humidity is observed, which tracks an increase of the ratio of the $(H_2O)NH_4^+$ and NH_4^+ ion signals (indicated by the color-code).

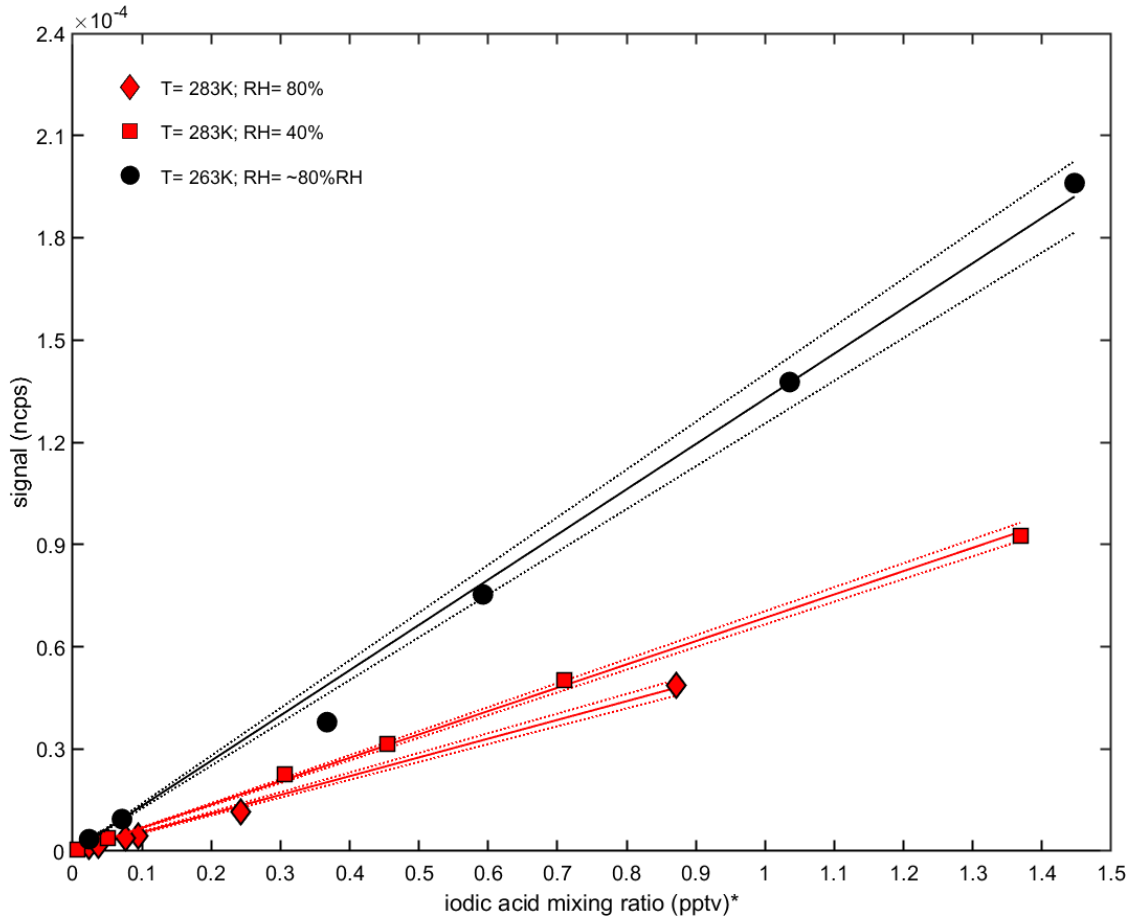

925 **Figure 6:** Calibration curves for iodic acid at different relative humidities and temperatures in the CLOUD chamber. The normalized counts per second (*y*-axis) are shown against the iodic acid mixing ratio measured with a nitrate CI-APi-TOF (*x*-axis). The sensitivity increases at lower temperatures (black line), while no strong dependency on relative humidity is found at 283 K (red line).

* Note that the iodic acid mixing ratio is derived by applying a calibration factor for sulfuric acid to the nitrate CI-APi-TOF data.

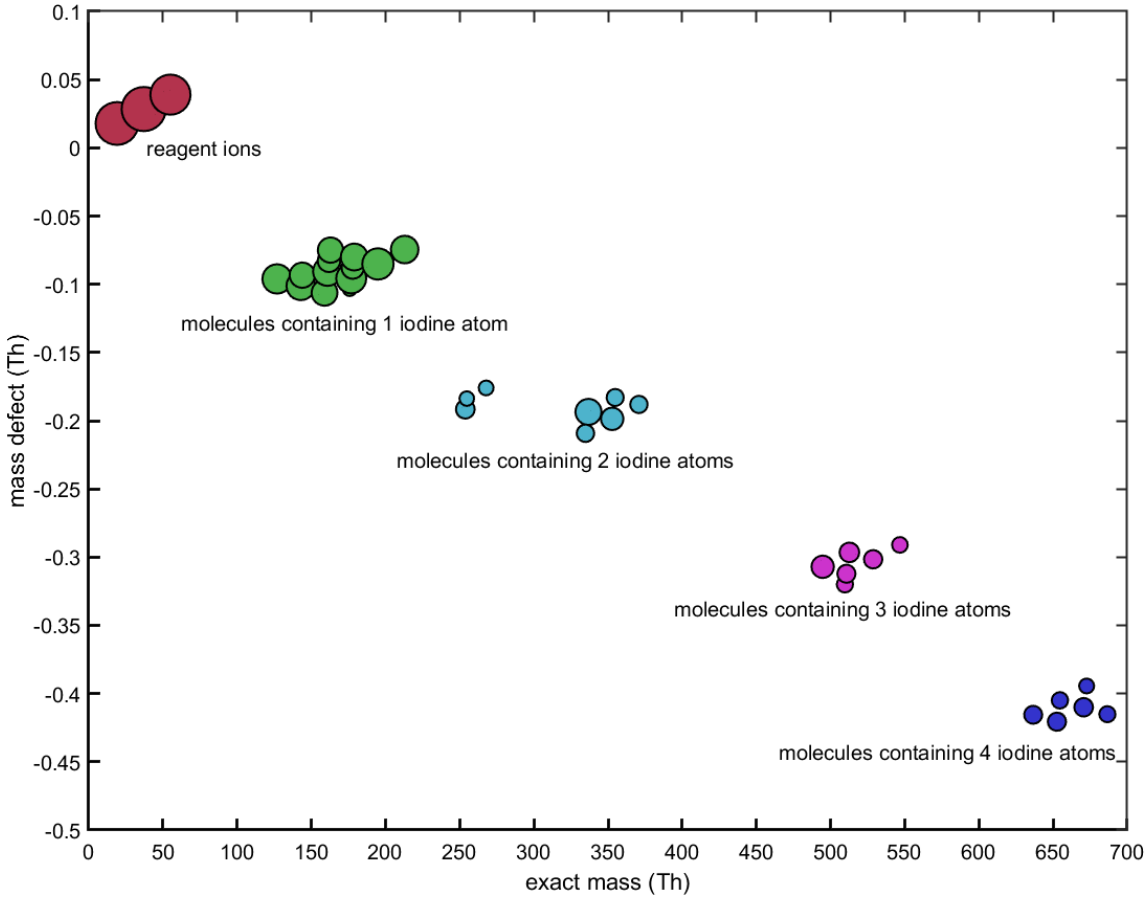

930

Figure 7: Mass defect plot for the iodine compounds, as well as the most prominent reagent ions, during a CLOUD experiment on new particle formation from iodine. The estimated iodic acid mixing ratio is ~0.98 pptv. The *y*-axis shows the mass defects of the compounds (see Table 2 and text for details), while the *x*-axis shows the absolute masses. The size of the symbols is proportional to the measured signal intensities on a logarithmic scale (from $1.24 \cdot 10^{-6}$ to 14.04 ions/s).

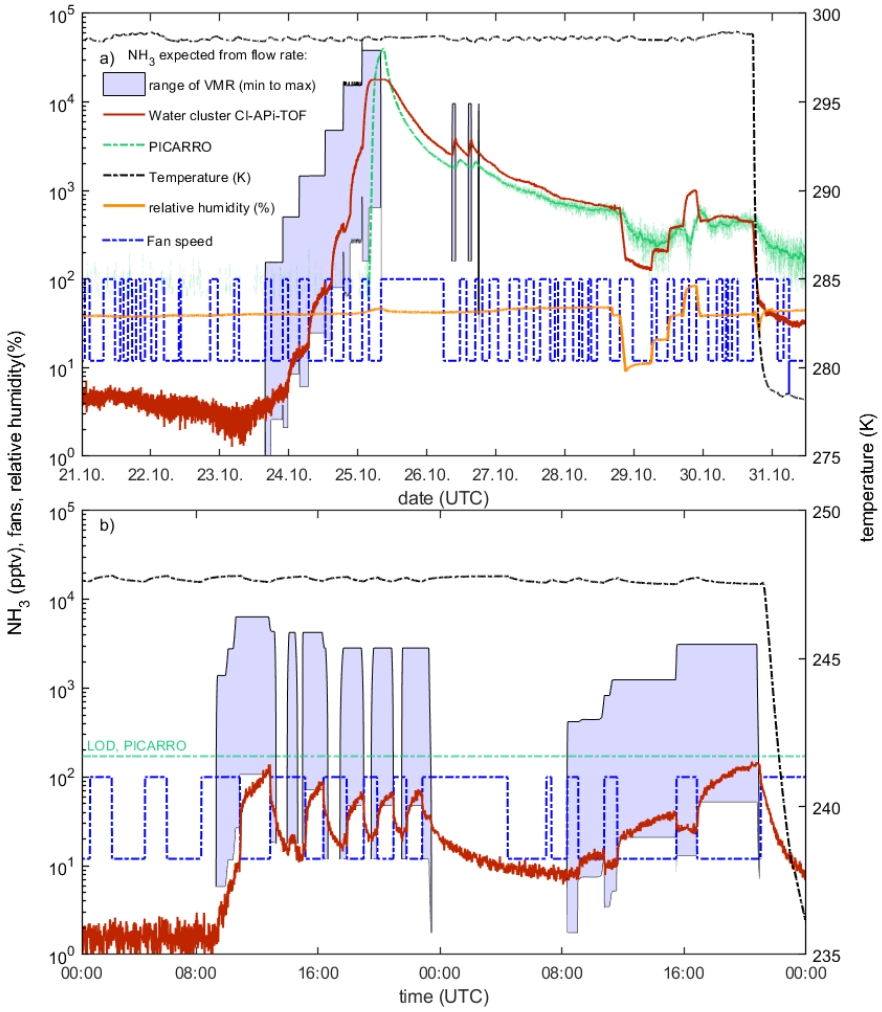

Figure 8: Inter-comparison between calculated (shaded blue area) and measured ammonia mixing ratios (PICARRO: solid green line; water cluster CI-APi-TOF: solid red line) at CLOUD. The PICARRO background (~200 pptv) has been subtracted, while no background was subtracted from the water cluster CI-APi-TOF. The temperature inside the chamber is indicated by the dashed black line. The speed (% of maximum, 397 revolutions per minute) of the two fans that mix the air inside the chamber is shown by the dashed blue line. The calculated ammonia mixing ratios (based on the calculated injection of ammonia into the chamber from the MFC settings) have a wide range due to uncertainties of the ammonia loss rate in the chamber. We display the maximum calculated range assuming, for the lower limit, that the chamber walls act as a perfect sink (wall loss dominated, 25 s and 100 s life time for fan speeds 100% and 12%, respectively) and, for the upper limit, no net uptake of NH_3 on the walls and a loss rate determined by dilution (6000 s life time). For higher fan speeds, the life time decreases due to increased turbulence and, in turn, increased wall loss rate. Relative humidity is indicated by the orange line. The water cluster CI-APi-TOF reacts rapidly to changing conditions, such as the ammonia flow into the chamber, relative humidity, temperature or fan speed. At low concentrations, the ammonia life time is determined by the wall loss rate (panel b and initial stages of panel a). However, at high ammonia concentrations, the walls of the CLOUD chamber progressively become conditioned and a source of ammonia, with

corresponding increases in the ammonia life time and the time to reach new equilibria at lower ammonia flow rates (later stages of panel a).

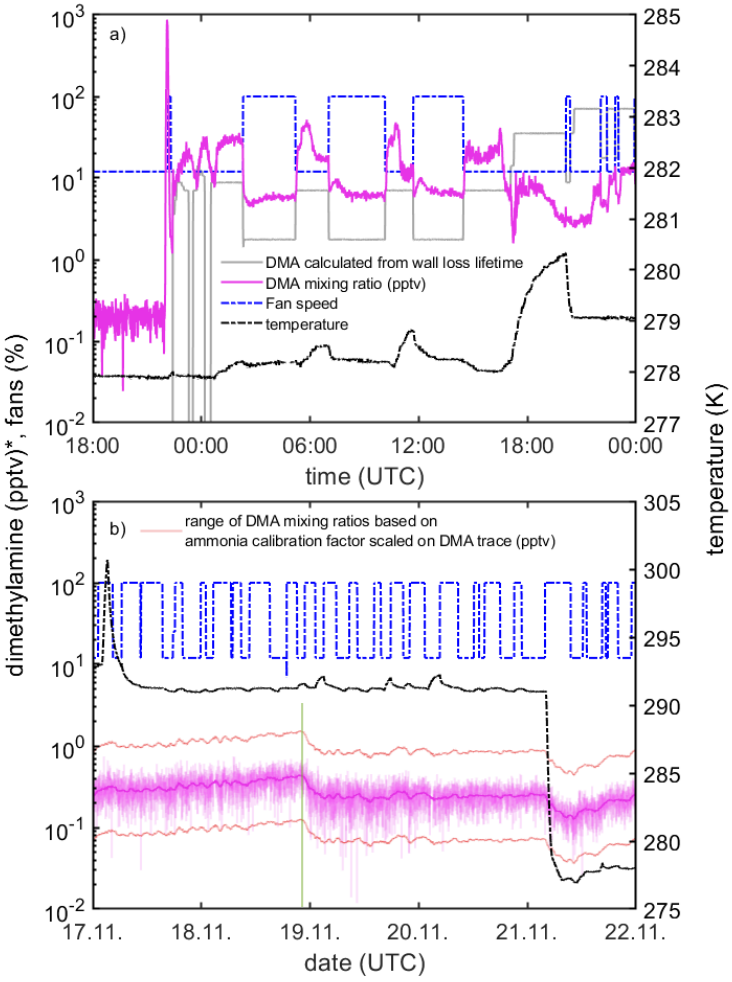

Figure 9: Dimethylamine mixing ratios (magenta line) during the CLOUD13 experiment. The dashed black line shows the temperature inside the CLOUD chamber. The dashed blue line shows the fan speed. Panel a) shows the dimethylamine signal during active injection into the chamber. The grey line indicates the dimethylamine mixing ratio in the chamber calculated from the MFC settings and the wall loss life time. The upper limit for the uncertainty in the dimethylamine mixing ratio is a factor of ~3.5 (see text for details). Panel b) shows a measurement of background dimethylamine in the chamber over a period of 5 days, when there was zero dimethylamine flow. We consider this to be due to instrumental background and not to an actual dimethylamine background in the chamber. The thin red lines show the possible range of dimethylamine based on the scaled calibration factor (factor 3.48, 95% CI). The thick magenta line indicates a moving average of the dimethylamine background measurement. The water source has been replenished during the period shown (green line). The mean instrumental background of dimethylamine over this period is ~0.14 pptv.

*Note that the dimethylamine mixing ratio is determined with the calibration factor for ammonia.